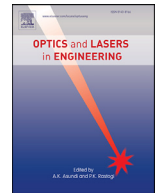




Contents lists available at ScienceDirect

Optics and Lasers in Engineering

journal homepage: www.elsevier.com/locate/optlaseng

Microscopic fringe projection profilometry: A review

Yan Hu^{a,b,*}, Qian Chen^a, Shijie Feng^{a,b}, Chao Zuo^{a,b}^a Jiangsu Key Laboratory of Spectral Imaging & Intelligent Sense, Nanjing University of Science and Technology, Nanjing, Jiangsu Province 210094, China^b Smart Computational Imaging (SCI) Laboratory, Nanjing University of Science and Technology, Nanjing, Jiangsu Province 210094, China

ARTICLE INFO

Keywords:

Three-dimensional sensing
Microscopic
Fringe projection
Optical metrology

ABSTRACT

Structured light three-dimensional (3D) measurement technology is considered one of the most reliable 3D data acquisition methods. Driven by the demand for high-precision 3D data acquisition for miniaturized samples in many fields such as surface condition analysis, mechanical function test, and micro-electro-mechanical systems (MEMS) quality inspection, microscopic fringe projection profilometry (MFPP) has been developed rapidly during recent decades. Significant progress has been made in different aspects of MFPP, including its optical configurations, corresponding system calibrations, phase retrieval algorithms, and 3D coordinate reconstruction methods. In addition, the rapid advance in high-frame-rate image sensors, high-speed digital projection technology, and high-performance processors become a powerful vehicle that motivates MFPP techniques to be increasingly applied in high-speed, real-time 3D shape measurement of dynamic samples. In this paper, we present an overview of these state-of-the-art MFPP works by analyzing and comparing the measurement principles, systems structures, and key performance indexes such as the accuracy, field of view (FOV), and speed. We also discuss the potential applications of MFPP and give some recommendations about optimum MFPP optical system design for reference in related applications in the future.

1. Introduction

The advances in electronic science and technology have continuously supported the development of the manufacturing industries. The emergence of a series of high-tech electronic products such as portable multimedia communication devices has profoundly affected people's lifestyles. In recent decades, industrial design has become more precise and miniaturized. Accordingly, the machining and fabrication standards have to meet more stringent constraints, which promotes the corresponding inspection techniques to develop in the direction of high precision, high efficiency, and low cost. Traditional quality inspection methods based on one-dimensional signals or two-dimensional images have failed to meet the requirements of modern industrial measurement for checking more details such as 3D data. As an approach to obtain the surface structure, 3D measurement plays an essential role in industrial processing and measurement, such as production line quality control, intelligent machine vision, reverse processing, auxiliary medical testing, and many other fields [1].

3D measurement can be divided into contact and non-contact methods. As to the contact measurement, one typical tool is the coordinate measuring machine (CMM) [2]. Its working principle is to perform the point measurement one by one and obtain the 3D coordinates by contacting the sensitive probe with the surface of the object, which has

micrometer-level measurement accuracy. However, for this method, the contact will produce interference on the targets. For the non-contact measurement methods, they can be divided into optical and non-optical categories according to whether or not using optical sensing to obtain information [3]. In this paper, the emphasis will be put on the optical sensing methods, which have the advantages of non-destructive, high accuracy, and high flexibility [4]. These methods can be roughly divided into photogrammetry, optical interferometry, structured light, etc.

Photogrammetry is a method of extracting and analyzing information from a picture taken by cameras. One typical method is the binocular vision, also known as stereo vision [5]. The difficulty of this method is to find the matching points when dealing with objects without apparent texture features [6,7]. Optical interferometry is widely used in refractive index measurement, distance measurement, and micro-deformation measurement [8]. Thanks to the continuous development of laser technology and precision optical processing technology, the interference fringes can be realized by a variety of methods, and correspondingly, the shear interferometry [9], speckle interferometry [10], and holographic interferometry [11] obtained rapid development. By extracting the phase of the interference fringe pattern, we can demodulate the wavefront information which is formed by the object and then restore the 3D shape of the object. However, these methods are based on optical interferometry that requires stable optical configuration and high-precision mechanical components, and the measurable objects are

* Corresponding author.

E-mail addresses: hu_yan@njust.edu.cn (Y. Hu), chenqian@njust.edu.cn (Q. Chen), zuochao@njust.edu.cn (C. Zuo).<https://doi.org/10.1016/j.optlaseng.2020.106192>

Received 6 December 2019; Received in revised form 31 January 2020; Accepted 11 May 2020

Available online xxx

0143-8166/© 2020 The Authors. Published by Elsevier Ltd. This is an open access article under the CC BY license. (<http://creativecommons.org/licenses/by/4.0/>)Please cite this article as: Y. Hu, Q. Chen and S. Feng et al., Microscopic fringe projection profilometry: A review, Optics and Lasers in Engineering, <https://doi.org/10.1016/j.optlaseng.2020.106192>

also limited to be with either high reflectivity or high transmittance. Though confocal microscopy using lasers as a light source has gained significant attention in recent years for its ability of super-resolution 3D measurements [12], its complex optical path structure makes it high-cost, and the measuring speed is still not efficient enough.

Another optical sensing method is the structured light projection, which uses a structured light source with specific geometric features to illuminate the object and uses the deformed structured light or image to restore the 3D shape of the object. As an active 3D measurement technology, structured light measurement has the advantages of smaller setup size, more straightforward processing, broader measuring range, and convenient installation and maintenance. According to the different measuring principles being used, structured light methods can be divided into two categories: time modulation and spatial modulation. More specifically, it includes the time-of-flight method [13], the direct triangulation method [14], the moiré fringe method [15], the phase measurement method [16], etc.

The phase measurement techniques using sinusoidal grating projection have been developed to improve the measurement resolution as well as the measurement efficiency. Phase measurement technique combines structured light projection technology with fringe analysis methods derived from interferometry to get 3D information of the object's surface by establishing a relationship between the surface height and the phase of the projected sinusoidal fringes. A digital fringe projection system generally contains two necessary devices - a projector and a camera, making the system cost-effective and easy to operate. According to the phase acquisition method, the phase measurement technique is divided into the Fourier transform profilometry (FTP) [16–18] and the phase-shifting profilometry (PSP) [19]. As a method for retrieving the phase maps based on spatial information, FTP only needs one or two fringe images, which is suitable for dynamic measurement and real-time monitoring while not ideal for surface measurement with large gradients. For PSP, a digital projection device is used to realize sinusoidal grating pattern projection with precise phase-shifting control. As PSP calculates the phase distribution point by point, it is insensitive to the color unevenness. Based on the calibrated phase-height relationship or the parameters of the camera and projector, we can calculate the 3D information of the object.

Since the advent of FPP [16], many scholars have done extensive researches focusing on different aspects of the fringe projection profilometry technique [20–24], covering binary pattern design [25–30], fringe sequence strategy [31–34], fringe projection speed [35–38], error analysis, and accuracy improvement [31,39–43], etc. At present, with the successful application of 3D measurement technology in various fields, its development mainly goes towards two directions. One direction is to the macroscopic measurement of large dimensional objects [38]. According to the application scenarios of 3D measurement using FPP in recent years, it can be seen that 3D measurement of macroscopic objects is very popular, and some commercial measurement systems, such as ATOS of GOM [44], FlexScan3D of polyga [45] also target the cameras with a regular FOV. The FOV of an FPP system depends on the spatial extent angle of the projected light and also the FOV of the camera. As the measurement distance increases, the FOV tends to increase, accompanied by the decrease of the projected light intensity and the decrease of the spatial resolution of the camera, which will reduce the accuracy of 3D measurements. According to the related reports, the measurement accuracy based on the traditional 3D FPP can reach 30–50 μm , which only meets the measurement requirements of macro scenes.

The other direction is to the microscopic measurement of smaller dimensional objects [46]. With the development of micro-machining technology that integrates multi-functional parts on tiny structural components, the MEMS has been widely applied to the fields of industrial processing and intelligent assembly [47]. However, advances in manufacturing technology are closely related to progressive measurement techniques, and measurement accuracy is also different when measuring objects in different FOV. Reviewing the various 3D measurement

methods over the years, they all face an inevitable compromise between the measurement accuracy and measurable volume size. In order to achieve high-accuracy measurement, the measurement volume needs to be correspondingly reduced. Therefore, how to take advantage of non-contact and full-field measurement features of FPP so as to achieve higher-precision measurement is a research topic with practical significance as well as technical challenges.

As the accuracy of 3D measurement has an inverse correlation with the size of the measured FOV, there is a feasible but not thoroughly studied method, known as the microscopic fringe projection profilometry (MFPP), which uses a microscopic optical path to shrink the projected pattern and imaging size. In contrast to conventional (macroscopic) FPP, the size of the target object to be measured with MFPP is usually much smaller, ranging from several centimeters to hundreds of micrometers. We can reduce the FOV of the projection and imaging by using a microscope or a lens with a long working distance (LWD).

In the projection unit, researchers have applied Ronchi gratings [48,49], liquid crystal display (LCD) [50], digital micromirror device (DMD) [51], and liquid crystal on silicon (LCoS) [52,53] as the fringe pattern modulator for MFPP systems. These attempts to project smaller patterns greatly promoted the development of MFPP. Compared with the well-known (macroscopic) FPP, the MFPP techniques did not get a similar level of attention at the early stage due to the following two main reasons:

- 1 The optical configuration of MFPP systems are generally more complicated, and the system calibration is also a tricky issue because additional lenses are introduced. Therefore, appropriate system configuration and relevant measurement theories are not well developed;
- 2 Due to the big optical magnification, MFPP setups have a much smaller FOV and shorter DOF compared with macroscopic FPP, making it can only measure micro-scale targets within a very short height range, like several millimeters.

However, as the development of optical and mechanical design capability, we are gradually able to build compact MFPP systems using miniaturized projectors with customized optical lenses. The emergence of high-speed and high-resolution digital light projectors also enables the phase-shifting of the fringe patterns to be controlled more accurately and flexibly [54]. Considerable progress has also been made in the camera calibration as well. Not only the pinhole model camera calibration method has been well developed [55], but the telecentric imaging model has also drawn enough attention [56], based on which a digitalized projector can even be calibrated and used as an inverse camera [22]. As microscopic measurements involve more optical components than only a traditional pinhole lens, related system calibration methods have been proposed [49,56–60], and the related real-time 3D measurement algorithms have also been developed rapidly [34,38,61–65]. All these have contributed to the development of MFPP, and without a doubt that MFPP will still play an irreplaceable role in the future 3D metrology because of its significant advantages of submicron-level accuracy, high flexibility, and low cost. Under such background, here we present a comprehensive review of the state-of-the-art MFPP approaches from several aspects, including the optical configurations, system calibrations, phase retrieval algorithms, and 3D coordinate reconstruction. We also discuss the potential applications of MFPP and give some recommendations about optimum MFPP optical system design for reference in related applications.

The following parts of this paper are organized as follows: In Section 2, MFPP systems based on stereomicroscopes are reviewed and followed by the review of MFPP systems based on LWD lenses in Section 3. In order to explain the basic principles regarding MFPP, we introduce some measuring principles used in 3D data retrieval in Section 4. The application of MFPP in real-time 3D measurement is introduced in Section 5, and in Section 6, we give some further discussion about MFPP, and the last section is the conclusion.

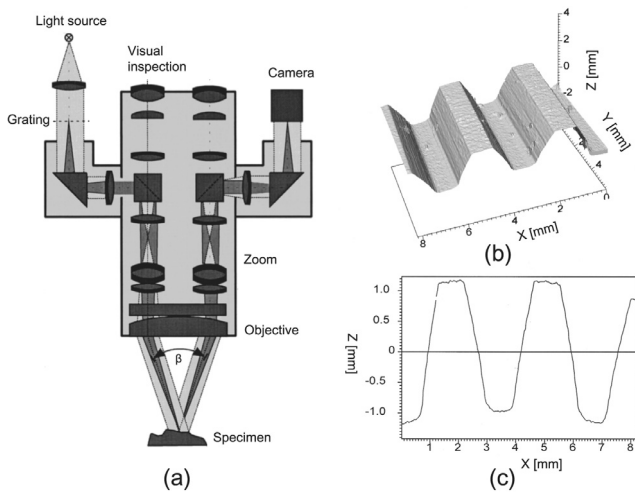


Fig. 1. 3D topometry using a stereomicroscope with a Ronchi grating-based fringe projection unit [49]: (a) schematic setup; (b) A retrieved 3-D topography a gear wheel; (c) A cross-section.

2. MFPP systems based on stereomicroscopes

2.1. Fringe pattern based on Ronchi gratings

The optical system configuration is one of the critical factors governing the complexity, flexibility, and stability of the 3D measurement. The earliest structured light projection microscopic 3D measurement technique employs half of the optical path of a microscope's objective as the projection light path and the other half as the imaging light path [48]. In this way, triangulation is formed under a micro FOV. The experimental results of this study prove that FPP can be built into a conventional microscope using the same aperture for illumination and detection to measure micro-shapes.

Later on, the research group of Windecker used two sub-optical paths of a common main objective (CMO) stereomicroscope as the optical path for projection and the imaging respectively to construct an MFPP system [49]. The structure of the system and a measurement result are shown in Fig. 1. The projected fringe is formed by illuminating a transmission Ronchi grating with a light source. The light passes through one optical path of the microscope and falls onto the sample after being changed the propagation direction by the edge portion of the shared objective lens. The light reflected by the sample passes through the other path of the microscope in the opposite direction, and the fringe modulated by the object surface finally imaged on the camera sensor. The topography is calculated by comparing the coordinates of the fringe image with respect to the coordinates obtained at a reference plane. A phase unwrapping method adapted from two-wavelength interferometry [66] is applied with two binary coded gratings. The system eliminates the need to retrofit a stereomicroscope and only requires the additional modular components to project fringe patterns into a relatively small FOV, which provides an effective solution for the application of FPP in the field of 3D microscopy.

Because the optical path of the microscope is encapsulated into an integral structure, the complete microscope can be mechanically translated in the vertical direction. Based on a similar setup as Fig. 1 (a), the one-grating projection for absolute 3D profiling is realized by finding the local peak of the modulation signal after low-pass filtering through z-scanning [67]. However, the fringe intensity is analyzed by assuming them as sinusoidal distribution, so it is necessary to project sinusoidal fringe patterns. The components for structured light projection in this system are composed of a point source and a binary grating. Although the grating can be optimized to make the grating closer to the sinusoidal model, it is still challenging to achieve the ideal sinusoidal fringe pro-

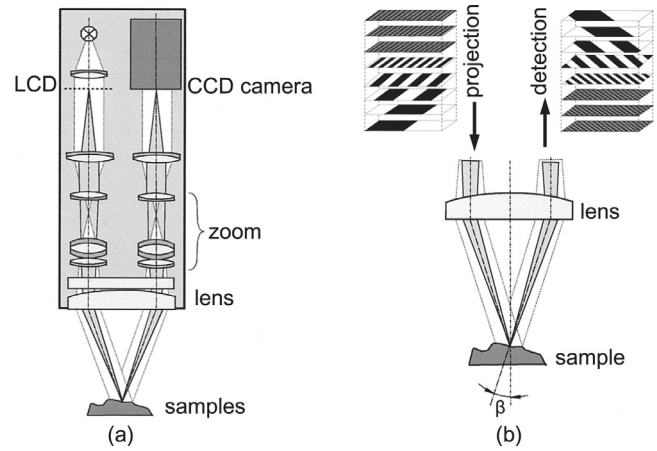


Fig. 2. An LCD based MFPP system [71]: (a) Setup of the stereomicroscope with an LCD-based pattern modulator; (b) Phase unwrapping by combining BGC technology and phase-shifting algorithm.

jection. At the same time, changing the projection pattern by replacing the grating also leads to low flexibility in measurement.

2.2. Fringe pattern based on optical modulators

With the development of two-dimensional optical modulation devices such as liquid crystal display (LCD) [68], digital micromirror device (DMD) [69], and liquid crystal on silicon (LCoS) [70], the generation of structured light becomes more flexible [4]. The projected pattern is generated by the computer and sent directly to the optical modulator. Based on these active optical modulators, researchers built many systems for MFPP.

Since the beginning of this century, LCD technology has stepped into maturity and been widely applied in the digital display area. It can change the transmittance of polarized light by actively changing the polarization direction of the crystal material to achieve multi-level grayscale pattern projection [50]. As shown in Fig. 2, Proll et al. [71] used an LCD panel instead of the binary Ronchi grating for micro FOV fringe projection, which can realize flexible pattern changes when the binary gray code (BGC) technology and phase-shifting algorithm are applied in the measurement of a German 1-pfennig coin.

Different from LCD based on transmittance modulation, a DMD chip has on its surface several hundred thousand microscopic mirrors arranged in a rectangular array which correspond to the pixels in the image to be displayed. The mirror is toggled on and off very quickly to produce greyscales, and the ratio of on-time to off-time determines the reflected intensity (binary pulse-width modulation). Zhang et al. [51] built a microscopic 3D shape measurement system with an expanded and collimated laser source, as shown in Fig. 3 (a). A DMD, along with its illumination optics, is integrated into a stereomicroscope. The measurement FOV ranges from 7.6 mm × 5.7 mm to 1.2 mm × 0.9 mm, depending on the zoom ratio in the tubes. However, each pixel of the DMD chip turns on or off by mechanically changing the mirror's angle; therefore, a precise arrangement is required to ensure the reflected light enters the microscope at a correct angle. The uniformity of the light source also needs to be guaranteed, so the system will be complicated in the design of the part of structured light illumination.

The projection technique using LCoS components enables structured light projection using a CMOS chip as a circuit substrate and reflective layer. It realizes patterns formation and projection by placing a beam splitter before the LCoS device. Proll et al. [53] reported on an application of a reflective ferroelectric LCoS as the fringe-generating element in a setup based on a stereomicroscope. Li et al. [52] also proposed a similar setup based on a stereomicroscope and LCoS, as shown in Fig. 4. After the LED light source is collimated, it is first reflected by the beam splitter

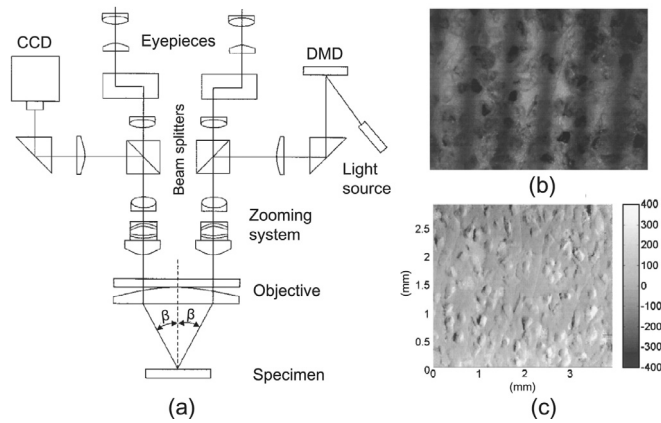


Fig. 3. A DMD based MFPP system [51]: (a) Optical layout of the fringe projection microscope system; (b) Fringe image; (c) Retrieved 3D shape of a piece of medium-grade sandpaper.

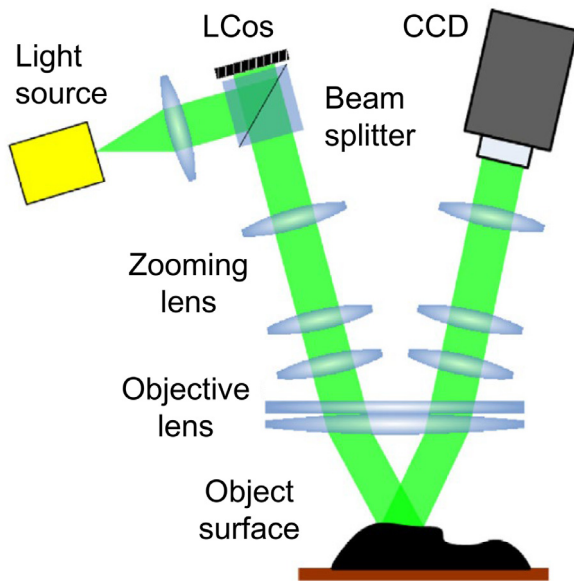


Fig. 4. An MFPP configuration based on a stereomicroscope and LCoS [52].

and irradiated to the surface of the LCoS. The modulated light forms a projected pattern, which passes through the beam splitter and enters the optical path of the stereomicroscope. LCoS projectors have better image contrast than LCD projectors and are more compact structure than DMD projectors. With this device, the depth resolution of measurements by use of phase-shifting algorithms can be significantly improved compared with the application of a Ronchi grating or an LCD.

2.3. Fringe pattern based on digital projectors

The focus plane of an ordinary digital projector is far from the lens, and thus the FOV of the projection is large because the FOV is proportional to the projection distance. Therefore, it is necessary to add a light path to reduce the FOV. As shown in Fig. 5, by adding an optical system to the front end of a commercial projector [72], the magnification of the pattern is reduced, and a large proportion of the pattern content can be projected into one optical path of the stereomicroscope to achieve microscopic pattern projection. However, due to the large size of a commercial projector, and the introduction of additional optical paths, the complexity of the entire measurement system will eventually be high.

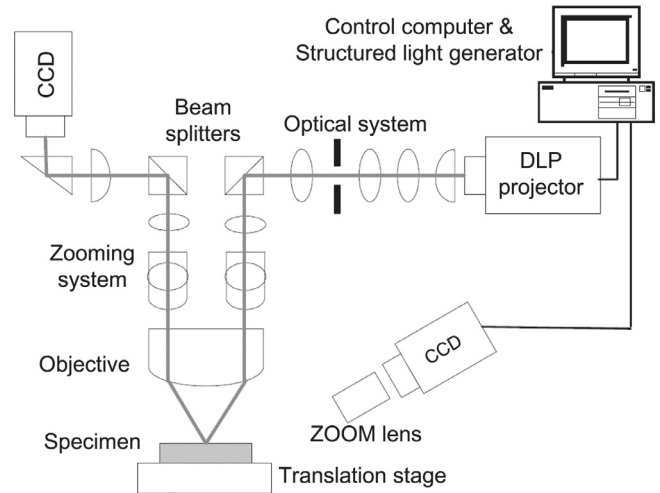


Fig. 5. An MFPP configuration based on a stereomicroscope and a commercial projector [72].

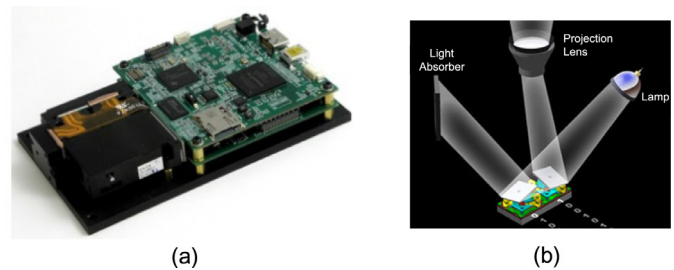


Fig. 6. (a) A commonly used miniaturized and versatile DLP Lightcrafter [54] and (b) its binary projection mechanism.

With the development of digital light processing (DLP) technology, Texas Instruments has launched a series of projection equipment for scientific research called DLP Lightcrafter based on its developed DMD technology. The product shown in Fig. 6 (a) is a commonly used DLP Lightcrafter model, which is miniaturized and versatile [54]. As mentioned above, each pixel's gray value depends on the ratio of on-time (1) to off-time (0), as shown in Fig. 6 (b). Compared with traditional commercial projectors, it has the advantages of smaller size, programmability, and easy to control, based on which high-speed structured light projection can be achieved [25,34,38,73,74].

Replacing a traditional commercial digital projection device with a DLP Lightcrafter to perform a microscopic 3D measurement can significantly reduce the system complexity. Yu et al. [75] present an MFPP system by using a stereomicroscope to generate a small-field projecting field and a DLP Lightcrafter to project the patterns into one eyepiece of the stereomicroscope directly, as shown in Figure 7. The system separately fixes the Lightcrafter and the CCD camera to mounting brackets other than the stereomicroscope, which results in the need to readjust the system arrangement when measuring samples at different heights and undoubtedly reduces measurement flexibility. This problem can be effectively solved by attaching the projector and the camera to the stereomicroscope, which requires the addition of connecting parts to allow the projector and camera to be fixed on the microscope body [58,76]. Consequently, the system need not be recalibrated when moving or measuring samples at different heights.

Jeught et al. [76] proposed a real-time microscopic profilometry system based on digital fringe projection and parallel programming. As shown in Fig. 8 (a), the Lightcrafter is fixed on the microscope, and the structured light patterns are projected onto an object through one pathway of a stereoscopic microscope. The algorithm timeline and snap-

Table 1
Comparison of MFPP systems based on off-the-shelf microscopes.

| Authors | Projection technique | System complexity | Year of publication | Measurement FOV |
|-----------------------|----------------------|-------------------|---------------------|---|
| Leonhardt et al. [48] | Ronchi grating | High | 1994 | $0.10 \times 0.10 \text{ mm}^2 - 2.50 \times 2.50 \text{ mm}^2$ |
| Windecker et al. [49] | Ronchi grating | High | 1997 | $1.40 \times 1.00 \text{ mm}^2 - 12.0 \times 6.50 \text{ mm}^2$ |
| Proll et al. [71] | LCD chip | High | 2000 | $1.40 \times 1.00 \text{ mm}^2 - 16.5 \times 12.0 \text{ mm}^2$ |
| Zhang et al. [51] | DMD chip | High | 2002 | $1.20 \times 0.90 \text{ mm}^2 - 7.60 \times 5.70 \text{ mm}^2$ |
| Proll et al. [53] | LCoS chip | High | 2003 | $0.83 \times 0.62 \text{ mm}^2 - 21.2 \times 15.7 \text{ mm}^2$ |
| Li et al. [52] | LCoS projector | Medium | 2013 | $3.0 \times 3.0 \text{ mm}^2$ (adjustable) |
| Chen et al. [72] | DLP projector* | Medium | 2005 | Not given |
| Yu et al. [75] | LightCrafter** | Medium | 2014 | $5.0 \times 5.0 \text{ mm}^2$ (adjustable) |
| Jeught et al. [76] | LightCrafter | Low | 2015 | $10.7 \times 8.0 \text{ mm}^2$ (adjustable) |
| Hu et al. [58] | LightCrafter | Low | 2017 | $8.0 \times 6.0 \text{ mm}^2$ (adjustable) |

*A DLP projector means a projector integrated with a DMD chip as the structured light modulator.

** A LightCrafter is a pattern-programmable projector based on the DMD technology.

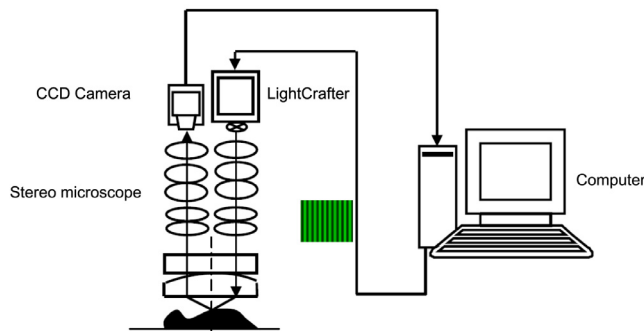


Fig. 7. An MFPP configuration based on a stereomicroscope and a DLP LightCrafter [75].

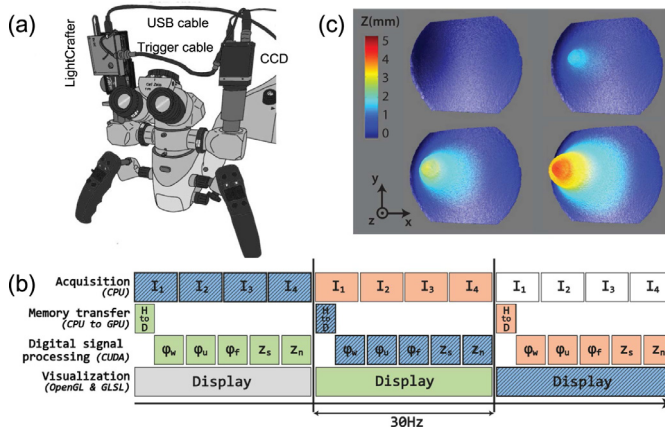


Fig. 8. A real-time 3D microscopic profilometry based on a CMO-type stereomicroscope [76]: (a) Optical setup; (b) Real-time four-step phase-shifting profilometry timeline; (c) Snapshots from a real-time 3D measurement video of a latex membrane.

shots from a real-time 3D measurement video are shown in Fig. 8 (b) and (c), respectively. Hu et al. [58] also present an optical configuration, in which a Greenough-type stereomicroscope arrangement is firstly applied in MFPP by using the coaxial optical paths of the stereomicroscope, as shown in Fig. 9. The difference is that a Greenough-type stereomicroscope is composed of two totally separate coaxial optical paths, while a single large objective shared by two optical paths can be found in a common main objective (CMO) type stereomicroscope.

The above-mentioned stereomicroscope-based MFPP systems have one thing in common, that is, they all use one of the two optical channels of a stereomicroscope for fringe projection and the other one for imaging. Each system has its pros and cons, and we summarized rele-

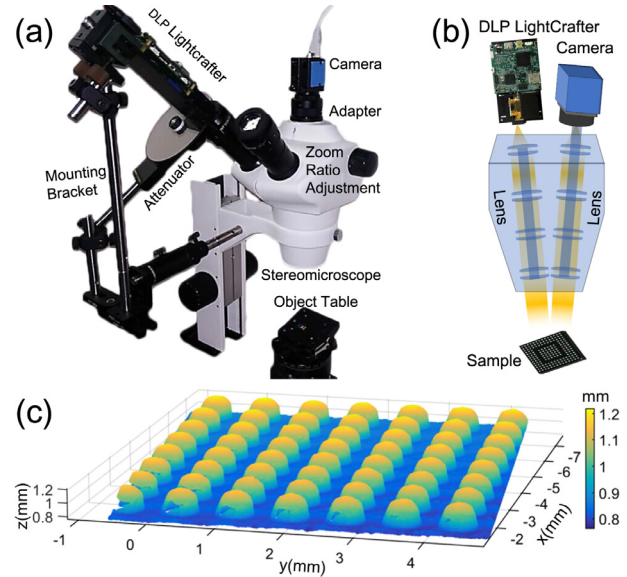


Fig. 9. A microscopic 3D measurement system based on a Greenough-type stereomicroscope [58]: (a) System setup; (b) Optical configuration; (c) A retrieved 3D result of a TFBGA.

vant information about these systems in Table 1. The considered aspects are the projection technique, system complexity, measurement FOV. We focus on the rationality of the system itself when comparing these MFPP systems. The algorithms used for these systems will be discussed in Section 4.

Notice the system complexity column in Table 1, if an independent optical element is used to modulate the intensity of the projected pattern [48,49,51,53,71], that will inevitably introduce a light path for the light source, so the system structure will become complicated. On the contrary, if a complete and compact digital projection unit, such as a digital projector, is used instead of a single active optical component to achieve structured light projection, both the stability and flexibility of the system will be significantly improved, as demonstrated in some works [52,72,75]. However, in their setups, the projector and the camera are not fixed on the microscope, which decreases the measurement flexibility when measuring samples at different heights. To make the system be able to cope with various measurement scenarios, an alternative way is to design special connectors to bind the projector and camera to the microscope [58,76].

When a stereomicroscope is used as the main body for MFPP, the advantage is that the FOV can be adjusted flexibly. The disadvantage is that the system volume is large, especially in the cases where additional optical components are introduced, which makes the system structure complicated and less stable. If we want to apply FPP more simply and

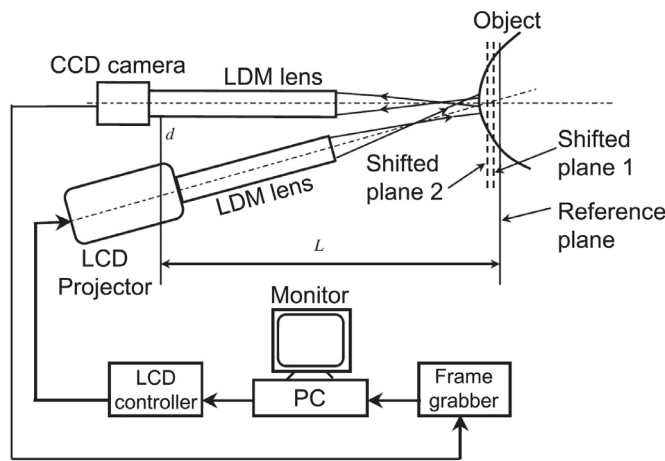


Fig. 10. An MFPP system based on LDM lenses [50].

stably to a microscopic environment, it is necessary to simplify the optical path, such as using LWD lenses with larger magnification and use appropriate calibration methods.

3. MFPP systems based on LWD lenses

Another kind of MFPP system uses an independent lens with a long working distance and a small FOV as the optical path [42,50,56,57,59,77–82]. To establish triangulation, the projection and imaging lenses need to form a certain angle, so the working distance of the lenses is required to be more than tens of millimeters to ensure that there is enough room to place the lenses, which means we need to use a lens with a long working distance (LWD). According to different imaging models, LWD lenses can be divided into non-telecentric lenses based on the perspective imaging model and telecentric lenses based on the affine imaging model [57]. Both lenses can achieve an FOV in millimeter-level.

The non-telecentric LWD lens has a long focal length to realize a large magnification, and a camera with a non-telecentric LWD lens can be calibrated using the pinhole model [55]. A telecentric lens is a compound lens that has its entrance or exit pupil at infinity, which can be divided into object-space telecentric lenses with an entrance pupil at infinity, image-space telecentric lenses with an exit pupil at infinity, and bi-telecentric lenses with both pupils at infinity. Because the camera's sensor is in the image side, we state here that the telecentric lens mentioned in this paper refers to the object-space telecentric lenses or the bi-telecentric lens because only these two kinds of telecentric lenses can achieve an image with a constant magnification over a certain depth in the image side.

3.1. One-camera MFPP systems

The structure of an MFPP system with only one camera is similar to a conventional FPP system. As shown in Fig. 10, by combining long working distance microscopes (LWDM) with an LCD projector, Quan et al. [50] realized microscopic surface profilometry based on the phase-shifting method. Because the projection and imaging light paths use separate lenses, the angle between the two paths is changeable. Some similar methods also use this kind of system structure [77–79]. The projection light path consists of a projector, an LWDM, and additional lenses in some cases, so the system structure is still complicated, and the phase-to-height fitting method is more suitable for 3D measurements compared with the pinhole-model based calibration method.

If we want to obtain the absolute 3D data of the target, we need to calculate all the points' positions in the Euclidean space. The most effective method is to solve the equations based on the camera imaging model

with unknowns being the point position in the world coordinate system [83]. Based on a DMD projector and two LWD lens, Yin et al. [80] built a system similar to Fig. 10 using the Scheimpflug principle to keep the focus plane of both light paths coincide at the object plane. A general imaging model is proposed by establishing the ray model corresponding to each pixel of the camera sensor and the DMD. 3D coordinates of the object point are obtained by solving the intersection coordinates of the two rays in space.

The emergence and development of telecentric lens calibration methods also promote the development of MFPP systems based on telecentric lenses [56,57,59,81,84–92]. Haskamp et al. [87] built an MFPP system using an object-space telecentric lens for the camera. Li and Zhang [57] used a bi-telecentric lens for the camera, and the projector with a pin-hole lens provides another view, based on which a 3D coordinate system in space can be established by separately calibrating the camera and the projector. Li et al. [59] built a system in which both the camera and the projector are equipped with a telecentric lens, as shown in Fig. 11 (a). Liu et al. [81] also used a similar setup to establish a 3D coordinate system, as shown in Fig. 11 (b). The difference between these two systems is the calibration method of the telecentric camera. Peng et al. [42] also built a setup composed of two telecentric lenses that are arranged according to the Scheimpflug condition, and a distortion correction method is proposed to correct all possible distortions induced by the Scheimpflug telecentric lens.

3.2. Multi-camera MFPP systems

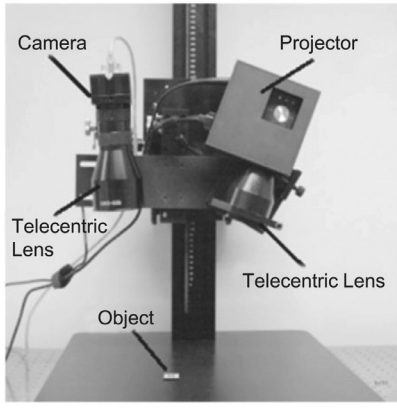
With the development of 3D reconstruction algorithms, multi-camera systems are gradually appearing and also get a lot of attention. By using more cameras in the microscopic environment, we can achieve complete measurement and extended depth of field (DOF) by merging 3D results from different perspectives [82], perform real-time 3D measurement with fewer fringe images [74,93], and apply more efficient calibration framework [56,82].

Since more than one camera is used, the final 3D data can be calculated from the matching points or disparity between multiple cameras instead of between the projector and camera. Based on Yin's calibration method [80], Wang et al. [82] built an MFPP system using a DMD chip and four cameras with LWD lenses to achieve 3D reconstruction based on the matching of the rays between two of the cameras. As shown in Fig. 12, the system can put the measurement ranges of the four cameras together to achieve an extended DOF and multi-views towards the target. Because the calibration of the projector requires a complicated back-projection processing stage, Hu et al. [56,74] proposed a new microscopic telecentric stereo vision system for 3D measurement, as shown in Fig. 13, in which the complicated projector calibration procedure can be avoided, and the phase maps calculated from the two cameras are rectified and referred to in the stereo matching.

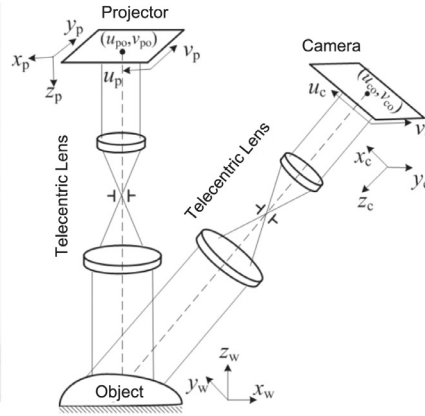
Here we summarize the relevant information of the MFPP systems based on LWD lenses, as in Table 2. The investigated factors contain the projection technique, LWD lens type, and measurement FOV. Since we have discussed the projection techniques in the last section, we do not focus on this part again. The flexibility of these systems is also very close; therefore, it is not considered, either. As to the accuracy, as we know, it is the most critical factor and depends heavily on the calibration and measurement algorithms, and this part will be reviewed in the next section.

4. The calibration and measurement methods of MFPP

In this section, we discuss the theoretical basis of the related technologies covered in this paper, including the basic principles of structured light projection, the implementation principle of phase retrieval, and the camera imaging model. Based on these principles, we review the calibration and measurement methods used in MFPP.



(a)



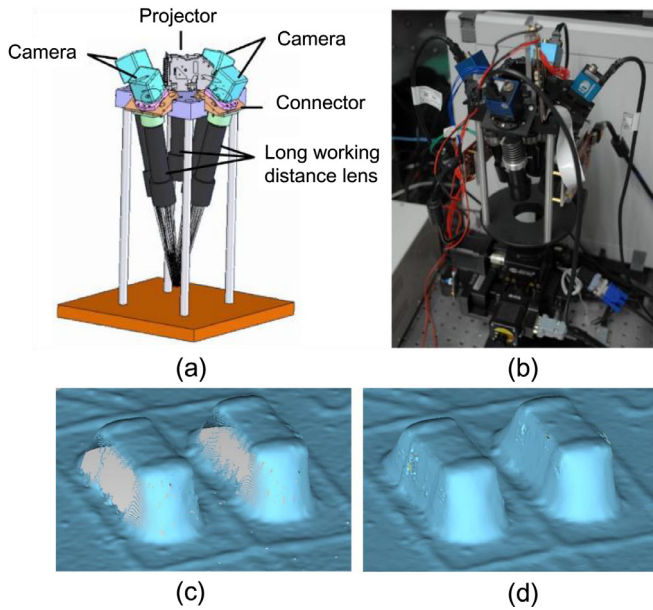
(b)

Fig. 11. MFPP systems based on telecentric projection and imaging: (a) The system picture in Ref. [59]; The measurement model of the FPP system with bi-telecentric lenses in Ref. [81].

Table 2

Comparison of MFPP systems based on LWD lens.

| Authors | Projection technique | Year of publication | LWD lens type (projector + camera) | Measurement FOV |
|-------------------|-------------------------|---------------------|--------------------------------------|----------------------------------|
| Quan et al. [50] | LCD projector | 2001 | Pinhole + Pinhole | $1.2 \times 1.5 \text{ mm}^2$ |
| Quan et al. [77] | Fine sinusoidal grating | 2002 | Pinhole + Pinhole | $0.1 \times 0.1 \text{ mm}^2$ |
| Wang et al. [78] | LCD projector | 2006 | Pinhole + Pinhole | $768 \times 576 \text{ pixel}$ |
| Chen et al. [79] | DLP projector | 2013 | Pinhole + Pinhole | Not given |
| Yin et al. [80] | DLP projector | 2015 | Pinhole + Pinhole | $5.0 \times 4.0 \text{ mm}^2$ |
| Li and Zhang [57] | LightCrafter | 2015 | Pinhole + Telecentric | $10.0 \times 8.0 \text{ mm}^2$ |
| Li et al. [59] | DLP projector | 2014 | Telecentric + Telecentric | $30.0 \times 20.0 \text{ mm}^2$ |
| Liu et al. [81] | LCD projector | 2017 | Telecentric + Telecentric | $34.6 \times 29.0 \text{ mm}^2$ |
| Peng et al. [42] | DMD chip | 2015 | Telecentric + Telecentric | $1280 \times 1024 \text{ pixel}$ |
| Wang et al. [82] | DMD chip | 2017 | Telecentric + $4 \times$ Telecentric | $1280 \times 1024 \text{ pixel}$ |
| Hu et al. [56] | LightCrafter | 2019 | Telecentric + $2 \times$ Telecentric | $10.0 \times 7.0 \text{ mm}^2$ |



(c)

(d)

Fig. 12. A four-camera MFPP system [82]: (a) The schematic design; (b) The photograph of the system; (c) and (d) are the 3D data from single view and multi-views of two surface mount components, respectively.

4.1. The basic principle of structured light projection

Different from the passive binocular 3D measurement technology [94], The structured light projection technique realizes binocular 3D measurement by actively illuminating the structured light to the object surface with coded information, such as phase, speckle, and stripes.

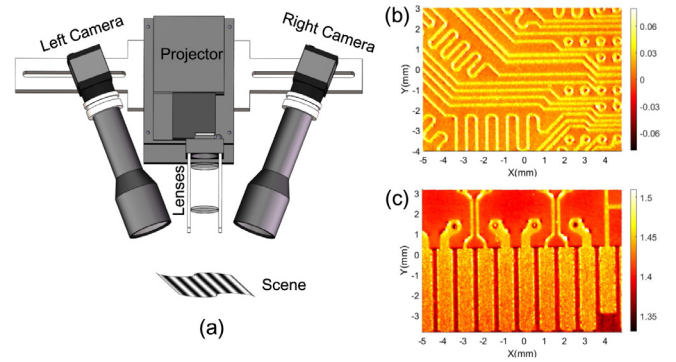


Fig. 13. A new microscopic telecentric stereo vision system: (a) Simplified system structure [56]; (b) and (c) are two top views of the reconstructed 3D data of electronic circuits and metal pads on a PCB, respectively.

A structured light projection system typically requires a digital pattern projection device and an image acquisition device. By using coded patterns, a projection device can assist in 3D measurement based on a binocular system. During the measurement, the structured light pattern is modulated by the surface topography of the object, and the fringe image is acquired by a camera. By performing phase decoding on one or several captured images, a mapping relationship between the points on the camera sensor and the original coded pattern can be obtained.

A simplified schematic diagram of the structured light projection technique is as shown in Fig. 14. One camera in a traditional dual-camera binocular system is replaced by a digital projector. O_P and O_C are the optical centers of the projector and camera light path, respectively. $O_P O$ and $O_C O$ indicate the optical axis direction of the projector and camera light path. l is the distance between the camera and the ref-

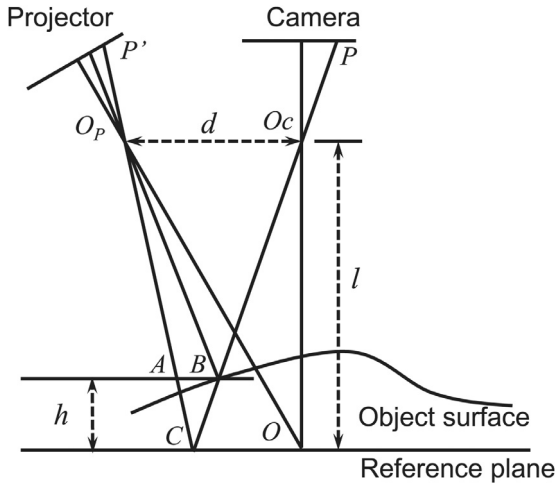


Fig. 14. A simplified schematic diagram of the structured light projection technique.

reference plane. d is the distance between the camera and the projector. h is the measured height relative to the reference plane. According to the geometric relationship in Fig. 14, we can deduce $\triangle ABC \sim \triangle O_P O_C C$, and thus we get a proportional expression

$$\frac{h}{l} = \frac{AB}{d} \quad (1)$$

According to Eq. (1), the length of h can be obtained by measuring the length of AB . Point P on the camera sensor corresponds to a different point P' on the projector plane when measuring different height objects. If we can get the matched position of the point P' , the length of AB can then be calculated [58,95]. The mapping relationship between P and P' is usually based on the phase value retrieved from the fringe images. The phase values can be converted to either the height or pixel coordinates on the projection plane. Anyway, the phase information extracted from the fringe patterns of the object is used as auxiliary information other than the monocular camera to obtain 3D information.

4.2. Phase retrieval method in FTP and PSP

Phase-coded sinusoidal or sinusoidal stripe-like patterns are most commonly used in 3D measurement, based on which the quantitative deformation of the fringe can be calculated. Phase retrieval methods were initially proposed to analyze the interference fringes produced by interferometry [96]. The typical interference fringe analysis method is the Fourier transform method [16–18], which processes the fringe image in the frequency domain. In recent years, with the emergence of various digital devices that can realize precise phase-shifting, the phase-shifting method has become widely used in fringe projection profilometry (FPP). This sub-section provides a brief introduction to the phase retrieval methods and the commonly used phase unwrapping algorithms in the field of FPP.

FTP was first proposed by Takeda et al. [16] for phase extraction from fringe images. By projecting a pattern with a higher fringe frequency on an object, the captured fringe image can be transformed into the frequency domain with several easily separated parts [97]. Thanks to the development of digital projection devices, the quality of the projection pattern has been dramatically improved. In the projection space, the fringe intensity can be expressed by

$$I_p(u_p, v_p) = a_p + b_p \cos(2\pi f_p u_p) \quad (2)$$

In Eq. 2, a_p is the averaged intensity, which is also called the background intensity. b_p is the fringe contrast, which is also called the fringe modulation. (u_p, v_p) is the coordinate of the projection device. f_p is the spatial frequency of the fringe. The fringe is distributed in the direction

perpendicular to u_p axis. After the pattern is sent to the projector and projected onto the object, it is captured by the camera. If the ambient light can be neglected, the captured image can be expressed as [36]

$$I_c(u, v) = a_c(u, v) + b_c(u, v) \cos[\Phi(u, v)] \quad (3)$$

Here, (u, v) is the camera's pixel coordinate, which can be omitted in the rest of this paper for brevity. $a_c(u, v)$ and $b_c(u, v)$ are the background intensity and fringe modulation, respectively. $\Phi(u, v) = 2\pi f_0 u + \phi_{obj}(u, v)$, and f_0 is the carrier frequency of the fringe. ϕ_{obj} is the modulated phase, which is the key factor containing the 3D information of the measured objects. Using Euler's formula, we can simplify Eq. (3) as the following exponential form

$$I_c = a_c + \frac{b_c}{2} [\exp(i\Phi) + \exp(-i\Phi)] \quad (4)$$

The 2D Fourier transform of Eq. (4) is

$$G(f_u, f_v) = A(f_u, f_v) + B(f_u, f_v) + B^*(-f_u, -f_v) \quad (5)$$

Here, $G(f_u, f_v)$, $A(f_u, f_v)$, and $B(f_u, f_v)$ are the Fourier transforms of I_c , a_c , and $(b_c/2)\exp(i\Phi)$, respectively. $B^*(f_u, f_v)$ is the complex conjugate of $B(f_u, f_v)$. Fourier shift theorem indicates that multiplying a carrier phase factor in the spatial domain is equivalent to a translation of the signal's spectrum in the frequency domain, so the three terms in Eq. (5) are separated to a certain extent in the Fourier domain. By using a windowed filter function, like a Hanning window [98], the $B(f_u, f_v)$ part corresponding to $(b_c/2)\exp(i\Phi)$ can be extracted. Applying the inverse Fourier transform to the extracted $(b_c/2)\exp(i\Phi)$, we can obtain the complex field with the phase component Φ included as

$$I_{inv} = b_c \exp(i\Phi) \quad (6)$$

Its corresponding wrapped phase ϕ can be obtained through

$$\phi = \text{angle}(I_{inv}) \quad (7)$$

Because FTP only needs one or two images, it is very suitable for dynamic 3D measurement [99].

Unlike FTP, which uses the entire fringe pattern for phase solving, PSP performs phase calculation for each pixel. In the case of using a digital projection device, the phase-shifting amount δ_n can be artificially changed. The fringe image with a shifted phase δ_n is changed from Eq. (3) to

$$I_n(u, v) = a(u, v) + b(u, v) \cos[\Phi(u, v) + \delta_n] \quad (8)$$

In addition to the known variables: δ_n and I_n , there are three unknowns, including a , b and Φ . Therefore, in order to calculate the unknowns, at least three phase-shifting images are required. Over the past few decades in FPP applications, many PSP algorithms have been proposed or extended from the field of PSI, for example, the standard N -step phase-shifting algorithm [100], double 3-step algorithm [101], Hariharan 5-step algorithm [102], modified 2+1 algorithm [103], trapezoidal phase-shifting [104], triangular phase shifting [105] and π -shift FTP [106] etc. Among these algorithms, the standard N -step phase-shifting algorithm is the most widely used because of its excellent performance in noise suppression [107]. In a standard N -step phase-shifting algorithm, $\delta_n = 2\pi(n-1)/N$, and we have N equations as

$$\begin{cases} I_1(u, v) = a(u, v) + b(u, v) \cos[\Phi(u, v)] \\ I_2(u, v) = a(u, v) + b(u, v) \cos[\Phi(u, v) + 2\pi/N] \\ \vdots \\ I_N(u, v) = a(u, v) + b(u, v) \cos[\Phi(u, v) + 2\pi(N-1)/N] \end{cases} \quad (9)$$

According to the least-squares algorithm [108], we can get

$$a = \frac{\sum_{n=1}^N I_n}{N} \quad (10)$$

and

$$b = \frac{2}{N} \sqrt{\left[\sum_{n=1}^N I_n \sin\left(\frac{2\pi n}{N}\right) \right]^2 + \left[\sum_{n=1}^N I_n \cos\left(\frac{2\pi n}{N}\right) \right]^2} \quad (11)$$

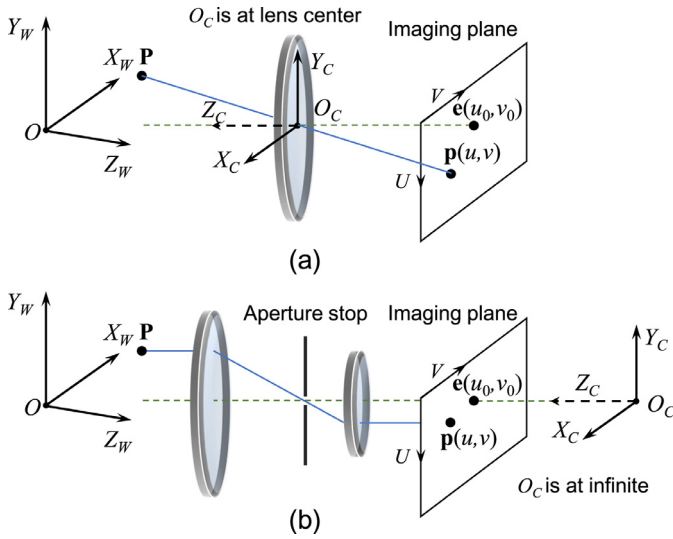


Fig. 15. (a) Pinhole imaging model; (b) Dual-telecentric imaging model.

as well as the wrapped phase $\phi(u, v)$ corresponding to $\Phi(u, v)$:

$$\phi = -\arctan \left[\frac{\sum_{n=1}^N I_n \sin \left(\frac{2\pi n}{N} \right)}{\sum_{n=1}^N I_n \cos \left(\frac{2\pi n}{N} \right)} \right] \quad (12)$$

However, due to the periodicity of the sinusoidal function itself, both the phase obtained by the FTP and PSP will appear in a wrapped form. The relationship between the wrapped phase ϕ and the unwrapped phase Φ can be expressed as [109]

$$\Phi(u, v) = \phi(u, v) + 2\pi k(u, v) \quad (13)$$

Here, k is the fringe order, indicating the number of 2π that needs to be compensated. The fringe order is the key parameter for many 3D reconstruction algorithms. The commonly used phase unwrapping algorithms are generally divided into two categories according to the implementation, namely, the spatial phase-unwrapping algorithm [41] and the temporal phase-unwrapping [42].

Spatial phase-unwrapping algorithms use only one wrapped phase map by judging the phase change of adjacent pixels in the spatial domain so that the effectiveness heavily depends on the phase unwrapping path [43]. Temporal phase-unwrapping algorithms realize the phase unwrapping according to the phases calculated from the combination of different fringes with different frequencies, which is an essential procedure to recover an unambiguous absolute phase even in the presence of large discontinuities or spatially isolated surfaces [109]. The effect of phase unwrapping depends not only on the quality of the wrapped phase itself but also on the choice of the number of fringe periods and the number of phase-shifting steps [33,32]. With the obtained phase map, we can perform stereo matching or phase-to-height transformation to get 3D data, but this is based on the known system parameters. Therefore, the system has to be mathematically modeled in some way, which will be discussed in the following sub-sections.

4.3. Pinhole and telecentric imaging models

The function of a camera can be understood as mapping a scene in a 3D world onto a two-dimensional image. 3D reconstruction is the reverse of this process. A pinhole and a dual-telecentric imaging model can be simplified, as shown in Fig. 15 (a) and (b), respectively. The imaging model depends on what kind of lens is mounted in front of the camera sensor.

Suppose a point $P(x, y, z)$ in the world coordinate is imaged on the camera sensor denoted as $p(u, v)$. We first introduce the pinhole model,

as shown in Fig. 15 (a). An ideal pinhole camera's imaging process can be represented as [55]

$$z_c \begin{bmatrix} u \\ v \\ 1 \end{bmatrix} = \mathbf{A} \mathbf{P}_C = \begin{bmatrix} f & 0 & u_0 \\ 0 & f & v_0 \\ 0 & 0 & 1 \end{bmatrix} \begin{bmatrix} x_c \\ y_c \\ z_c \end{bmatrix} = z_c \begin{bmatrix} x_c f / z_c + u_0 \\ y_c f / z_c + v_0 \\ 1 \end{bmatrix} \quad (14)$$

Here, \mathbf{A} is the intrinsic matrix. f is the focal length, which is the distance between O_C and $e(u_0, v_0)$. (u_0, v_0) is the center pixel coordinates. $\mathbf{P}_C(x_c, y_c, z_c)$ is the point coordinate in the camera's coordinate system, and is obtained by multiplying \mathbf{P} by the rotation matrix \mathbf{R} plus the translation matrix \mathbf{t} :

$$\mathbf{P}_C = \mathbf{R} \mathbf{P} + \mathbf{t} = \begin{bmatrix} r_{11} & r_{12} & r_{13} \\ r_{21} & r_{22} & r_{23} \\ r_{31} & r_{32} & r_{33} \end{bmatrix} \begin{bmatrix} x \\ y \\ z \end{bmatrix} + \begin{bmatrix} t_x \\ t_y \\ t_z \end{bmatrix} \quad (15)$$

The ideal imaging process of the other kind of camera, telecentric camera, as shown in Fig. 15 (b), can be represented as [56]

$$\begin{bmatrix} u \\ v \\ 1 \end{bmatrix} = \mathbf{A} \mathbf{P}_C = \begin{bmatrix} m & 0 & u_0 \\ 0 & m & v_0 \\ 0 & 0 & 1 \end{bmatrix} \begin{bmatrix} x_c \\ y_c \\ 1 \end{bmatrix} \quad (16)$$

Here, m in the intrinsic matrix \mathbf{A} is the lens' equivalent magnification, which combines the optical magnification and pixel size. The difference in \mathbf{P}_C between two imaging models is that z_c in a telecentric camera is omitted because a telecentric camera is not sensitive to the depth changing in its optical axis [84].

Many calibration methods for both types of cameras have been proposed [110–112,55,56,83,85,86], based on which quantitative 3D reconstruction can be realized with multi-vision setups. In FPP, one vision is usually replaced by a digital projector to project active phase-coded patterns on the target. From the captured fringe images, the phase is used as the intermediate variable of 3D measurement.

In FPP, 3D reconstruction methods can be divided into two categories: parameter fitting [58,113–116] and stereo-matching [22,56]. Parameter fitting methods usually require a standard object containing known 3D information [95,115], or a plurality of planes that are parallel to each other with known distance [58,76]. Stereo-matching methods used in 3D reconstruction are to find the stereo matching pixels from two or more perspectives [22,42,56], which can be either the projector or cameras. For one-camera systems, one perspective is usually provided by a projector that replaces a camera in a traditional binocular vision.

4.4. 3D measurement based on phase-to-height relation

The height distribution of an object causes the deformation of the fringes, which changes the phase values of fixed points. Based on a specific mathematical model, we can convert the phase value or phase deviation into a height value. There are many proposed methods used to calibrate the phase-height relation through global parameters [58,60,113–117]. Phase or phase deviation and height are in a linear relationship when certain conditions are met; that is, the fringe density is evenly distributed in space. This condition needs the projected optical path to be telecentric [60].

The length of AB in Fig. 1 can be obtained by counting the number of periods in the fringe image [49,53]. However, many commercial digital projectors are equipped with a pinhole lens so that the simple relation in Eq. (1) is not appropriate for accurate and absolute 3D measurement. Another problem is that the coaxiality of the optical path has to be satisfied as a primary condition in order to use the pinhole model. Even though many pinhole lens calibration methods are developed, the optical path of microscopes is non-coaxial, such as the non-coaxiality between the optical path of the microscope and the lens of the projector [58] and the non-coaxiality inside a CMO microscope between the horizontally mounted objective lens and the two obliquely mounted eyepieces. The non-coaxiality makes it difficult to calibrate the optical path using standard matrix models.

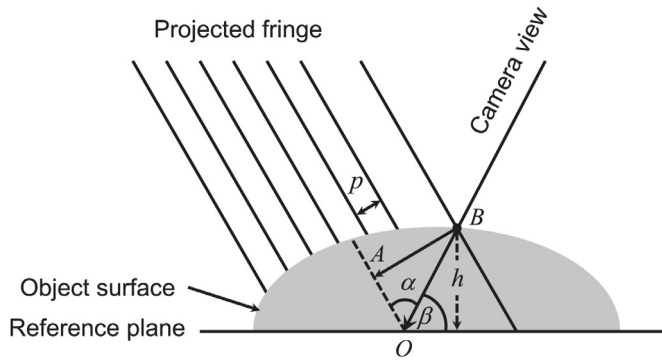


Fig. 16. Simplified geometry for telecentric illumination.

However, stereomicroscopes have a long focal length, which makes the microscopes have quasi telecentricity. By assuming the fringe pattern is evenly distributed after being projected through the microscope, the height of the sample is calculated based on the linear transformation of the phase deviation with the equivalent wavelength in the measurement plane [49–51,53,76]. As shown in Fig. 16, the angle between the camera view and the projection direction is α . The angle of the camera view is β . AB is perpendicular to the projection direction. $\Delta\Phi_{AB}$ is the phase deviation between the reference phase and measured phase, based on which the length of AB can be obtained by $\overline{AB} = p\Delta\Phi_{AB}/2\pi$, where p is the fringe pitch. The height of the point on the camera can be calculated by

$$h = \overline{AB} \frac{\sin \beta}{\sin \alpha} = p \frac{\Delta\Phi_{AB}}{2\pi} \frac{\sin \beta}{\sin \alpha} \quad (17)$$

Because the angle of the camera view and the projection angle are almost fixed owing to the telecentricity of the microscope, the height and phase are linearly related. However, when the fringe pattern is generated and projected by additional lenses, the telecentricity can no longer be maintained. As more accurate and flexible fringe patterns are needed in modern microscopic 3D measurement, digital projector becomes inevitable in MFPP [50,52,58,72,75,76,81]. Many setups are built with a projector that has its own projection lens. Besides, the telecentricity of a stereomicroscope is by no means perfect. In order to analyze the light path with an ideal model, the non-linear phase-to-height transformation needs to be developed.

Nevertheless, almost the proposed methods are used in macro-scale 3D measurement, and they can be divided into global parameter-based methods [114,115,117] and local parameter-based methods [58,113]. Global parameter-based methods are derived from pinhole camera models, which means the optical path of such kind system has to be coaxial. Take the actual situation into account that many MFPP systems are based on non-coaxial systems, local parameter-based methods for the phase-to-height calibration are proposed. Hu et al. [113] introduced a geometrical analysis method into a stereomicroscope based MFPP system to set up a relation between the unwrapped phase and depth locally [58]. In this method, all the light rays are modeled as lines in 3D space. As shown in Fig. 17, $O-XYZ$ denotes the world coordinate system. UV is defined in the CCD plane, and $X_G Y_G$ is defined in the DMD plane. $O_P - X_P Y_P Z_P$ is the projector coordinate system, and $O_C - X_C Y_C Z_C$ is the camera coordinate system. $O_C O_C'$ and $O_P O_P'$ are the optical axis of the camera and the projector, respectively. H and H' mean the principal points of the microscope part. The optical distortion is also corrected, based on which the absolute and accurate 3D data can be obtained combined with the calibrated camera model.

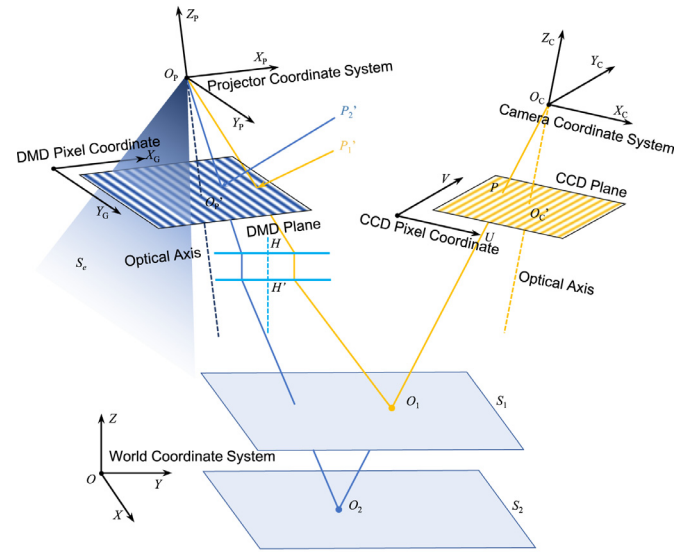


Fig. 17. Schematic diagram of the optical path model based on a stereomicroscope.

Phase-to-height is, however, a partial step towards the ultimate 3D data because only the depth information z is acquired. There is also lateral information containing x and y need to be calculated. In the system proposed by Liu et al. [113], after modeling the geometrical ray to obtain the relationship between the phase and height, the lateral position is calculated by establishing the relationship between the fringe pitch and the phase at different heights. This method obtains the 3D coordinates in the projection coordinate system. However, due to the perspective distortion of the optical path, the horizontal plane of the world coordinate and the projection optical axis must be perpendicular to each other. Zhu et al. [60] proposed to use a linear transformation between image unit (pixel) to the metric unit (mm) by assuming that the magnification along the x or y direction is constant, which is workable under telecentric imaging.

With the development of digital projectors and pinhole calibration algorithms, a digital projector can also be calibrated as an inverse camera; thus, the phase map coded in the fringe patterns can help stereo matching in an MFPP system, which will be introduced in the next subsection.

4.5. 3D measurement based on imaging models

As we have introduced above, lenses that can be used in microscopic 3D measurement must have a small FOV but an extended DOF. The limited DOF of the long-distance microscope lens limits the measurement range, especially in the depth dimension, so telecentric lenses are more appropriate for this requirement. In this subsection, 3D measurement approaches by using telecentric lenses are reviewed. The most important part is the telecentric camera calibration itself because telecentric camera calibration algorithms are still not developed as mature as the algorithms used for pinhole cameras. Therefore, the telecentric camera calibration algorithms are firstly reviewed here for a complete introduction to the MFPP based on imaging models.

Many proposed systems use telecentric lenses to increase the measurement volume [57,59,60,87]. As we introduced in Section. 4.3, the imaging model corresponding to the telecentric camera corresponds to an affine transformation, which is unlike the conventional pinhole camera model that is based on perspective transformation. Both the internal parameter matrix and the external parameter matrix of these two models are different due to the insensitivity of the telecentric camera to the position variation along its optical axis. Scholars have car-

ried out a series of methods on the calibration of telecentric lenses to improve the accuracy and flexibility, and significantly improved the measurement efficiency of the telecentric lenses based systems [42,84–86,88,92].

Li et al. [85] proposed a telecentric lens calibration method and used it in a telecentric microscopic 3D measurement system composed of a digital projector and a camera. In this calibration method, a plane with 2D comb function distributed circles is applied as the calibration target. A neglected issue is that the depth insensitivity of a telecentric lens in the direction of the optical axis leads to uncertainty of the pose of the plane, which makes the extrinsic matrix of the imaging model difficult to determine [118]. To solve this problem, Chen et al. [92] proposed a method of obtaining the image of the calibration target in a shifted position by a translation stage to help determine the normal direction of each calibration pose. Li et al. [57] proposed an MFPP system that includes a long-distance lens for the projector and a telecentric lens for the camera. The pixel coordinates of the feature points of the projector's light path are obtained by the phase-shifting method. Then the relative position of all the calibration poses can be obtained, thereby providing the 3D coordinates of all the feature points of all calibration poses, which also solves the pose ambiguity problem.

However, if the projected FOV needs to be shrunken further, the valid projection DOF with good fringe contrast would be much shorter. For the system in which the optical paths and all telecentric, Liu et al. [81] used a 3D model as the calibration target and uses factorization method and beam adjustment to realize the calibration of the telecentric microscopic 3D measurement system. Yin et al. [80] calibrated an MFPP system based on two LWD microscope lenses through three calibration poses. This method first obtains the external parameters of each pose through three patterns and uses the feature points on the calibration pattern as the constraint condition to establish a ray-tracing model between each pixel on the camera sensor and the projection chip, which is named general imaging model.

Summarizing the calibration and measurement method in those mentioned microscopic 3D measurement systems, we can divide them into two categories according to the type of lens used, that is, systems using long-distance microscopic lenses and systems using telecentric lenses. The former is a perspective model and is easy to calibrate, but because the measurable DOF is limited, it is impossible to perform 3D measurement of the space outside the valid DOF. The latter is an affine model that can provide a more extended DOF but requires complicated calibration methods. Especially when calibrating the projector, complex phase coding fringe projection is often required to inversely map the coordinates of the object space to the pixel coordinates of the projection space. In order to avoid the complex and unstable calibration of the projector and effectively utilize the characteristics of a large DOF of a telecentric camera to realize flexible and accurate microscopic 3D measurement, Hu et al. [56] proposed an MFPP based on epipolar rectification of a telecentric stereovision system. A telecentric camera calibration algorithm involving the distortion center estimation is also proposed. The complexity of the dense stereo matching process is greatly simplified by applying accurate telecentric calibration and rectification for the stereovision system.

Here we summarized the calibration and measurement methods of MFPP systems as well as the accuracy and FOV that are provided in these papers, as listed in Table 3. Although similar fringe patterns are applied in all MFPP systems, the phase retrieval algorithms may be different. Besides, the criteria for the measurement error in these works are different. In some works, it is to measure a plane to see the root-mean-square (RMS) error. Also, some methods try to see the deviation between the retrieved depth and the preset position. These two ways are all based on plane measurement, which is 2D but not the absolute 3D error. The actual 3D measurement should be in the 3D space. However, the accuracy of any dimension still shows some particular effectiveness of the corresponding method. About the comparison and discussion about phase calculation and unwrapping

algorithms, the readers can refer to another two review papers [19,109].

5. Real-time microscopic 3D measurement and potential applications

5.1. Optimization of fringe patterns used in MFPP

In the phase retrieval based 3D measurement, whether it is based on Fourier transform or phase-shifting algorithm, using high-frequency fringes is an effective method to increase the measurement range and the measurement accuracy. To guarantee reliable phase unwrapping, we need to increase the phase-shifting step or use more intermediate fringe frequencies with additional auxiliary patterns. Consequently, the measurement efficiency will be reduced accordingly. In recent years, FPP techniques based on Fourier transform and phase-shifting have been developed a lot [99,19], as well as the phase unwrapping methods [109]. However, for these various methods, the actual system parameters are not considered to optimize the fringe frequency and the number of patterns as well. It is necessary to design an appropriate fringe pattern combination for a particular system according to its system parameters. Therefore, whether Fourier transform or phase-shifting is used, it is necessary to establish a fringe optimization method for a known system: designing an optimal combination of patterns or maximizing measurement accuracy with a limited number of patterns.

With different frequencies used in FTP, the fringe ambiguity can be solved, and high-speed measurements can also be realized. It has been demonstrated that by using high-frame-rate projection hardware, accurate, denser, unambiguous, and motion-artifact-free 3D reconstruction at speed up to 10,000 Hz can be realized by μ FTP method [35]. The temporal phase unwrapping algorithm used in the μ FTP method is called projection distance minimization (PDM), in which multiple wavelengths are used to solve the phase ambiguity optimally in the maximum-likelihood sense. However, Li et al. [33] found that the choice of the wavelengths is essential to the unambiguous measurement range as well as the unwrapping reliability in the presence of noise, and a qualitative conclusion is given that the noise resistance ability of PDM is fundamentally determined by the value of each item in wavelength ratio: a smaller value of each item in wavelength ratio means better noise resistance ability in phase unwrapping.

For phase-shifting based binary pattern optimization, Hu et al. [25] proposed a method that effectively combines optimized binary structured patterns with a number-theoretical phase unwrapping algorithm to realize real-time microscopic 3D measurement. The spectral of the binary pattern is studied, and a binary pattern optimized method is developed to cooperate with the spectral characters of phase-shifting algorithms. A slight defocusing of the optimized binary patterns can considerably alleviate the measurement error based on four-step phase-shifting FPP, providing the binary patterns with comparable performance to ideal sinusoidal patterns.

5.2. Acceleration of computation

In order to calculate the phase from the real-time acquired fringe images and reconstruct the 3D result in high-speed. The computer is required to provide superior computing power. For this reason, the fast processing method for fringe projection has been greatly developed [25,41,119–123]. Usually, real-time measurement requires several steps: image acquisition, image preprocessing, such as denoising, rectification, distortion elimination, then phase calculation, stereo matching, and finally, the reconstruction and display of 3D data. Although these steps usually are performed sequentially, pipelined and multi-thread technology can be used to accelerate the whole process [34,76], thus increasing the temporal resolution of the 3D measurement. In terms of phase calculation, GPU acceleration technology can significantly increase the processing speed by parallel computing and significantly re-

Table 3
Calibration and measurement methods of MFPP systems.

| Authors | Optical basis | Calibration method | Measurement method | Measured accuracy (FOV) | Projection technique |
|-----------------------|------------------|-------------------------------|----------------------------------|--|----------------------|
| Windecker et al. [49] | Stereomicroscope | Phase-height relation | Two-grating phase-shifting | 2.5 μm rms ($8 \times 5 \text{ mm}^2$) | Ronchi grating |
| roll et al. [53] | Stereomicroscope | Phase-height relation | 4, 5, 8-step phase-shifting | 0.085 μm rms ($1.04 \times 0.77 \text{ mm}^2$) | LCoS chip |
| Proll et al. [71] | Stereomicroscope | Phase-height relation | Gray-code+3-step phase-shifting | Not given | LCD chip |
| Zhang et al. [51] | Stereomicroscope | Phase-height relation | 3- step phase-shifting | 2.6 μm p-p variation (1.2 mm) | DMD chip |
| Li et al. [52] | Stereomicroscope | Pinhole model | Multi-frequency phase-shifting | 3.1 μm ($3 \times 3 \text{ mm}^2$) | LCoS projector |
| Chen et al. [72] | Stereomicroscope | Pinhole model | Triangulation | Below 1% (of full-scale) | DLP projector |
| Yu et al. [75] | Stereomicroscope | Phase-height relation | 4-step phase-shifting | Not given | LightCrafter |
| Jeught et al. [76] | Stereomicroscope | Phase-height relation | 4-step phase-shifting | 17 μm isometric error ($10.7 \times 8.0 \text{ mm}^2$) | LightCrafter |
| Hu et al. [58] | Stereomicroscope | Phase-height relation | Multi-frequency phase-shifting | 1.2 μm rms ($3 \times 3 \text{ mm}^2$) | LightCrafter |
| Quan et al. [50] | LWD lenses | Phase-height relation | 4-step phase-shifting | 2.5% discrepancy ($2 \times 1.5 \text{ mm}^2$) | LCD projector |
| Wang et al. [78] | LWD lenses | Phase-height relation | 4-step phase-shifting | 18 μm ($768 \times 576 \text{ pixel}$) | LCD projector |
| Chen et al. [79] | LWD lenses | Phase-height relation | 5-step phase-shifting | 18.1 μm (Not given) | DLP projector |
| Yin et al. [80] | LWD lenses | General imaging model | Gray-code+16-step phase-shifting | 4 μm std ($5.0 \times 4.0 \text{ mm}^2$) | DLP projector |
| Li and Zhang [57] | LWD lenses | Pinhole+telecentric model | Multi-frequency phase-shifting | 4.5 μm rms ($10.0 \times 8.0 \text{ mm}^2$) | LightCrafter |
| Li et al. [59] | LWD lenses | Telecentric model | Multi-frequency phase-shifting | 5 μm std ($30.0 \times 20.0 \text{ mm}^2$) | DLP projector |
| Liu et al. [81] | LWD lenses | Telecentric model | Gray-code | 10 μm rms ($34.6 \times 29.0 \text{ mm}^2$) | LCD projector |
| Peng et al. [42] | LWD lenses | Scheimpflug telecentric model | Gray-code+4-step phase-shifting | 2 μm max ($1280 \times 1024 \text{ pixel}$) | DMD chip |
| Wang et al. [82] | LWD lenses | General imaging model | Not given | 0.6 μm std ($1280 \times 1024 \text{ pixel}$) | DMD chip |
| Hu et al. [56] | LWD lenses | Telecentric model | Multi-frequency phase-shifting | 1.4 μm std ($10.0 \times 7.0 \text{ mm}^2$) | LightCrafter |

duce the working pressure of the CPU, which otherwise executes the codes in serial order. In some time-consuming operations, we can use the lookup table [124–126] technique to reduce instruction cycles, and thus the amount of computation is decreased. In addition, with the development of various third-party code libraries, like Point cloud library (PCL), Open graphics library (Open GL), Open computing language (Open CL), Open source computer vision library (Open CV), etc., the point cloud results can be calculated in higher speed, displayed diversified and operated freely.

5.3. Application of real-time MFPP

Under the premise of using the same measurement method, if more measurement data is obtained, the extracted phase value tends to be more accurate. However, in some measurement situations, it is often necessary to complete a 3D measurement in the shortest time, especially real-time 3D measurement requirements [36,61,127,128], and even transient measurement [35]. In practical applications, the fast 3D measurement can be divided into two specific application scenarios according to different image capture speed. The first scenario requires both the image acquisition and 3D reconstruction in a short period by using high-speed hardware. This kind of situation focuses on the absolute accuracy of the measurement. During the projection process, the measured object is required to be statically placed. We can increase the number of projected fringe patterns to get a more accurate phase reconstruction [58]. Synchronous projection and capture sequences with hardware trigger signals ensure that data will not be aliased during the fast image acquisition stage.

The other scenario needs to continuously measure, record, and display the 3D shape of a dynamic object over time. Since its purpose is to

obtain a continuously changing topography, it focuses on improving the frame rate of both projection and camera. In addition to this, it is necessary to reduce the measurement data (the number of fringe patterns) to a considerable extent to reduce the measurement error introduced by motion [129]. Although continuous measurement can provide real-time shape detection and recording, it is often challenging to obtain ideal measurement results because of the motion.

A popular method for improving measurement efficiency is using FTP to calculate the fringe phase [16]. The conventional algorithm in FTP is similar to the phase analysis method in interferometry in which a higher fringe frequency is preferred. The Fourier translation theory shows that multiplying the spatial domain signal by a carrier frequency factor is equivalent to the frequency shift in the frequency domain. Therefore, three mutually separated sub-spectral regions - a zero-frequency portion and two mutually conjugated primary frequency portions, appear in the fringe spectrum domain. However, when measuring complex object topography, the zero frequency and the primary frequency part are prone to aliasing in the spectrum domain, especially when the carrier frequency of the fringe is not high enough. In order to solve this problem, the π -shift FTP (π FTP) method was proposed to eliminate the zero-frequency portion in the spectrum by additionally projecting a fringe pattern that is π out of phase with the original pattern and subtracting the two fringe patterns [130,131]. Since the phase information from π FTP is obtained by two sinusoidal patterns with a phase shift, it is still sensitive to motion. To solve this problem, another improved FTP (Modified FTP, MFTP) was proposed by projecting another uniform intensity pattern to eliminate background effects [132]. Hu et al. [73] proposed a marker embedded FTP (MEFTP) in the real-time microscopic 3D measurement by using specially designed markers in two patterns to absolutely unwrap the phase map.

In addition to FTP, we can calculate the phase by projecting phase-shifting fringes at high speed. However, in the application of real-time MFPP, there are not too many related works being reported. Jeught et al. [41] used the graphics processing unit (GPU) acceleration technology to achieve a height map measurement speed of 30 frames per second by using a four-step phase-shifting algorithm (Fig. 8). For a faster measurement speed, the projection mechanism based on multi-bit binary pattern integration is no longer appropriate. Li et al. [64] built a 3D microscopic profilometry system to perform high-speed microscopic 3D measurement with a binary defocusing technique, and a frame rate of 500 Hz is achieved. A nine-step phase-shifting algorithm is employed because binary fringes have more high-order harmonics than the ideal sinusoidal fringes, and thus more phase-shifting steps need to be used to reduce the measurement errors introduced by higher-order harmonics. Therefore, how to effectively utilize the high-speed projection advantage of binary fringes and effectively avoid the influence of high-order harmonics in the microscopic environment with small DOF is a subject worthy of further study. Hu et al. [25] proposed a real-time microscopic 3D shape measurement based on optimized pulse-width-modulation binary fringe projection, in which a strategy to generate optimized pulse-width-modulation patterns with frequency components suitable for the property of the four-step phase-shifting algorithm is presented. The binary fringe patterns generated by this strategy can provide measurement accuracy comparable to that of ideal sinusoidal fringes.

To summarize the difference between real-time MFPP and traditional FPP, we mainly focus on two points. The first one is the calibration and measurement difference caused by the system structure. The second one is how to apply appropriate phase retrieval algorithms by taking advantage of the small FOV in the microscopic environment to increase the accuracy. Other than these two points, the other parts of both the real-time MFPP and traditional FPP are nearly the same. Compared with traditional FPP techniques, MFPP techniques show their advantages of higher measurement adaptability to different scales of targets, but this does not mean it is trouble-free. To thoroughly discuss the characteristics from various aspects of MFPP, we still need to discuss some unsolved or need-to-improve parts regarding MFPP, which is discussed in Section 6.

5.4. Application in on-line quality control

MFPP is very useful in the quality control of high-end manufacturing. Some inferior-quality products may have some very tiny defects or cracks in the processing. The defective part is likely difficult to distinguish in the traditional observation way because of the accuracy level may be unable to meet the demand. MFPP can be applied to detect these defects owing to its high-precision 3D measurement when other methods, such as laser interference, are not qualified because of the material limits of the targets.

Nowadays, the micro-scale components, like MEMS, have very big demands for high-accuracy 3D imaging to check their dynamic mechanical properties. As the real-time MFPP develops, on-line quality check of micro-level can be easily realized in industrial target detections. We believe that MFPP will play a huge role in the industrial field and even become an irreplaceable 3D measurement method.

5.5. Application in high dynamic range measurement

In a microscopic environment, it is often to measure the surface of materials with high reflectivity. There are mainly two types of techniques that can optimize the measurement results for such problems. One type is based on changing the projection light intensity or based on multiple exposure techniques [133–135]. The other is to optimize the phase reconstruction results by specific algorithms on the raw data [136–138]. The former method is more complicated for operation because it needs to adjust the projection and capture parameters several times, and is only suitable for offline measurement scenes. Therefore,

it is more suitable for fast measurement scenarios by using the appropriate algorithm for phase optimization at a later stage. In fact, for the microscopic optical path, different fringe density causes different fringe contrast because of the limited DOF of the lenses, and thus the saturation area may be different if the fringe density is different. Hu et al. [139] proposed to calculate phases of these highlighted areas from a subset of the fringe sequence, which is not subjected to the intensity saturation. By using the proposed multi-frequency phase-shifting scheme, the integrity of the 3D surface reconstruction can be significantly improved. The ultimate phase maps obtained from unsaturated intensities are used to achieve high-accuracy 3D recovering of shiny surfaces based on a phase stereo matching method.

6. Further discussions

6.1. Single-camera versus multi-camera

According to the current application of FPP systems, it is required to use a single structured light projection device (a projector), but the number of cameras varies. As the 3D data requires at least two viewing angles, in most situations when performing partial area measurement, one camera plus one projector can fulfill the requirements. In particular, for microscopic 3D measurements based on a stereomicroscope which has only two separate optical paths, we have to adopt the single-camera solution by using one of the optical paths for projection and the other optical path for imaging. The increasing demand for measurement also promotes the development of measurement systems. When the single-camera system cannot complete the measurement from different orientations simultaneously, it is necessary to introduce a multi-view or multi-camera solution. More cameras can provide 3D data from different depth or multi-angles simultaneously so that we can enlarge the measurable volume by superimposing the data. However, the system calibration method of multi-camera systems still requires to be further studied to ensure the efficacy of 3D data registration.

6.2. Scheimpflug photography for larger measurement volume

In the microscopic optical path, we want to get a DOF as long as possible, which does not need to be considered in the case of conventional macro FOV measurements. Although the DOF of telecentric lenses is better than others, they still need to fulfill the requirement of larger volumes. In a system based on multi-views, if the nominal imaging plane of the projector does not coincide with that of the camera, the measurement volume of the entire system will be reduced. In the MFPP system based on telecentric lenses, one solution is to this problem to use the Scheimpflug principle to align the projector's object-side projection volume with the camera's object-side imaging volume. The advantage of the Scheimpflug-based dual-telecentric high-frequency system makes it significant in the high-precision measurement with large-field cameras, but as to its calibration and rectification methods, further research is required.

6.3. Considerations of optical characteristics

Most of the reviewed MFPP systems in this paper have an FOV of a few millimeters. Depends on the target size, one can select the optical path with the appropriate magnification. Systems based on telecentric lenses have to change the lenses with different magnifications, while the magnification of a stereomicroscope can be adjusted freely, but after adjustment, the system must be recalibrated.

The essence of MFPP is no more than to reduce the fringe pattern to a smaller FOV, so the ratio between the phase error and the metric error increases accordingly. That is to say that the same phase error will result in less measurement error. However, it is necessary to pay more attention to the particularity of the microscopic optical path. Based on the spatial geometry, the smaller the FOV is, the higher the accuracy

Table 4
Comparison among DMD, LCD, and LCoS projectors.

| Item | DMD | LCD | LCoS |
|----------------|-----|-----|------|
| Brightness | ✓✓✓ | ✓✓ | ✓✓ |
| Black level | ✓✓✓ | ✓✓ | ✓✓✓ |
| Contrast ratio | ✓✓ | ✓✓ | ✓✓✓ |
| Speed | ✓✓✓ | ✓ | ✓ |
| Dimensions | ✓✓✓ | ✓✓ | ✓ |
| Cost | ✓✓✓ | ✓✓ | ✓✓ |
| Color accuracy | ✓✓✓ | ✓✓ | ✓✓ |

is. However, when the FOV is quite small, the lens must have a large enough numerical aperture to capture a clear image, which requires the object to be placed very close to the lens and is unfeasible for the optical path arrangement. Even for a commercial stereomicroscope with compact optical paths, it can image sharp imaging at millimeter level FOV only.

In practical MFPP system design, the contrast of the projected fringe is more important than the resolution because the period of the sinusoidal fringe is much larger than the optical resolution. However, when the projected light is converged into the small FOV, the light energy will also be more concentrated, causing the fringe brightness to exceed the limit of the camera's dynamic range, for example, intensity saturation occurs even with minimal exposure time. To solve this problem, we can use a lens with an adjustable aperture. This is because, on the one hand, changing the projection aperture can change the projection brightness; on the other hand, the DOF of the projection path can also be enlarged by reducing the aperture, which leads to high-contrast fringe projection in a deeper depth range.

The FOV of the projection light path must be larger than that of the camera to ensure the fringe is full in the camera's FOV, but cannot be too large; otherwise, the accuracy and density of the fringe will be affected. Then an optimized method is using a lens with an adjustable focal length for the projector. There may be concerns about the cost of the lens; actually, once the parameters are determined in the lab, the cost can then be reduced in mass production if needed. Besides, it is also necessary to pay attention to the physical size of the camera sensor and projector chip (DMD or LCD) as well as the target size to select appropriate optical paths. Assuming that the measurement range is 10 mm × 10 mm and the chip size is 4 mm × 6 mm, then the lens magnification is at least 2.5 times to make sure the projected patterns cover the target area.

6.4. Choice of digital projectors

Structured light projection is inseparable from a digital projector. The projector is better to project designed coded patterns accurately, quickly, and without distortion. DMD, LCD, and LCoS projectors are commonly used, and we make a simple comparison of their characteristics here. Note that it focuses on several core parameters related to structured light projection and the conclusion is not absolute as the technology is continuously moving forward, so when it comes to specific devices, situations may differ from what is described.

As shown in Table 4, DMD based projectors have the best brightness level and black level because of the mirror-reflection mechanism and thus have a good contrast ratio and give more realistic images. DMD can project patterns very fast, but when color patterns are used, researchers should use projectors with multi-DMD or multi-LED [54] to avoid rainbow artifacts [140].

LCD projectors have higher power efficiency and the best color reproduction [141]. The panels of LCD projectors do not have any moving parts, which ensures that the projector does not suffer from mechanical failure. However, LCD projectors have the lowest contrast ratio. They are not able to display text as clearly as DMD or LCoS projectors [142].

LCoS projectors also have excellent contrast ratio thanks to their hybrid technology, based on which they can output better and sharper images than both DMD and LCD projectors. The refinements in LCoS technology have ensured that the brightness is acceptable for most cases. For more comparison between LCoS and DMD projectors in generating digital sinusoidal fringe patterns, readers can refer to [143].

Other performance comparisons, such as dimensions, cost, and color accuracy, are also listed in Table 4. From the above analysis and comparison, it is found that DMD projectors have the most outstanding overall performance. Combined with the programmable features [54], DMD projectors are the most popular projection equipment for scientific researchers, especially for high-speed digital pattern projection.

6.5. Other recommendations

The performance of the whole system that needs to be concerned can be summarized as accuracy, speed, data density, measurement volume, and the diversity of software function. Currently, the core challenge is to improve the measurement accuracy, which is relying heavily on the calibration accuracy. However, due to the small-size of FOV in MFPP systems, standard targets used for micro FOV calibration is not easy to produce. If we want to obtain a measurement accuracy of sub-micron, the surface of the calibration plate is required to be very flat; therefore, it is necessary to fabricate or process high-precision calibration patterns on transparent glass.

Some features of the optical path of an MFPP system have been analyzed in the previous subsection, so in this part, only the features and some basic functions of the other parts in the system are discussed. The projection device is better being able to control the data depth of the pattern image in order to realize high-speed projection. Stable timing is the fundamental guarantee for reliable data acquisition, so the exposure duty cycle and the period need to be adjusted to meet the exposure requirement of the camera. Besides, there should be no gamma effect during pattern projection, and as known to us, the Lightcrafter based on DMD technology is the best device that can fulfill these requirements.

Camera devices theoretically require the pixel size to meet requirements of the optical resolution. Typically, in the telecentric and stereomicroscope optical paths, the optical resolution of the imaging side is limited by the small numerical aperture; therefore, the pixel size of several microns has already met this requirement. Another consideration is the pixel number, which decides the data density. For real-time measurement, the large amount of data will decrease the 3D frames per second, so the data processing techniques are essential.

Regarding the basic optical system, there are two possible solutions: stereomicroscopes and telecentric lenses. Stereomicroscope-based systems are more suitable for height measurement because the coefficient fitting method can achieve a phase-height relationship. However, it is often difficult to characterize the accurate optical path models, making the reliability of measurement unguaranteed. In recent years, related papers present more systems using telecentric lenses because the optical path can be freely set, and the optical path is very compact, making it more suitable for absolute 3D measurement. In terms of the complexity of the calibration, the binocular telecentric structure seems to be a better choice because it can realize high-precision 3D reconstruction without calibrating the projector, which undoubtedly reduces the workload of the system calibration.

7. Conclusions

In this paper, we have reviewed the development of MFPP, a microscopic 3D profilometry technique, which aims to achieve high-precision 3D measurement in a small FOV by combining FPP with a microscopic optical system. Accordingly, two kinds of systems for achieving of the high-precision measurement have been reviewed, namely, stereomicroscope-based and telecentric lenses-based systems. The corresponding system calibration and the reconstruction algorithms are dis-

cussed, and the advantages and disadvantages of different system configurations are detailedly compared. Besides, some techniques and applications of real-time 3D measurements based on microscopic optical path characteristics have also been reviewed. Finally, some further discussion and recommendations have been provided. We hope this review could provide comprehensive technical or methodological references for practitioners of MFPP and provide valuable insights into the design of a suitable MFPP measurement solution to a specific engineering problem.

Declaration of Competing Interests

The authors declare that they have no known competing financial interests or personal relationships that could have appeared to influence the work reported in this paper.

Acknowledgments

This research was funded by National Key R&D Program of China (2017YFF0106403), National Natural Science Fund of China (61722506, 61705105, 111574152), Final Assembly "13th Five-Year Plan" Advanced Research Project of China (30102070102), Equipment Advanced Research Fund of China (61404150202, 61404130314), The Key Research and Development Program of Jiangsu Province, China (BE2017162), Outstanding Youth Foundation of Jiangsu Province of China (BK20170034), National Defense Science and Technology Foundation of China (0106173), Six Talent Peaks Project of Jiangsu Province, China (2015-DZXX-009), 333 Engineering Research Project of Jiangsu Province, China (BRA2016407), Fundamental Research Funds for the Central Universities (30917011204, 30916011322), Open Research Fund of Jiangsu Key Laboratory of Spectral Imaging & Intelligent Sense (3091801410403, 3091601410414), China Postdoctoral Science Foundation (2019M661843), Special Project on Basic Research of Frontier Leading Technology of Jiangsu Province of China (BK20192003).

References

- [1] Chen F, Brown GM, Song M. Overview of 3-D shape measurement using optical methods. *Opt Eng* 2000;39:10–23. doi:10.1117/1.602438.
- [2] Raab S. Three dimensional coordinate measuring apparatus. US5402582A, 1995.
- [3] Abramovici M, Emmert JM, Stroud CE. Roving STARS: an integrated approach to on-line testing, diagnosis, and fault tolerance for FPGAs in adaptive computing systems. In: Proceeding third NASADoD workshop evolvable hardware EH-2001; 2001. p. 73–92. doi:10.1109/EH.2001.937949.
- [4] Gorthi SS, Rastogi P. Fringe projection techniques: whither we are? *Opt Lasers Eng* 2010;48:133–40. doi:10.1016/j.optlaseng.2009.09.001.
- [5] Lazaros N. Review of stereo vision algorithms: from software to hardware. *Int J Optomechatronics* 2008;2:435–62. doi:10.1080/15599610802438680.
- [6] Derpanis KG. The harris corner detector. York Univ 2004.
- [7] Ke Y, Sukthankar R. PCA-SIFT: a more distinctive representation for local image descriptors. *Comput Vis Pattern Recognit 2004 CVPR 2004 Proc 2004 IEEE Comput Soc Conf On 2004;2 IEEEII–II*.
- [8] Creath K. Phase-measurement interferometry techniques. *Prog Opt* 1988;26:349–93.
- [9] Steinchen W, Yang L. Digital shearography: theory and application of digital speckle pattern shearing interferometry 2003;93 vol..
- [10] Jones R, Wykes C. Others. Holographic and speckle interferometry, 6. Cambridge University Press; 1989.
- [11] Kreis T. Holographic interferometry: principles and methods. *Simul Exp Laser Metrol Proc Int Symp Laser Appl Precis Meas Held Balatonfured Hungary 1996;2:323*.
- [12] Pawley J. Handbook of biological confocal microscopy. Springer Science & Business Media; 2010.
- [13] Cui Y, Schuon S, Chan D, Thrun S, Theobalt C. 3D shape scanning with a time-of-flight camera. *Comput Vis Pattern Recognit CVPR 2010 IEEE Conf On, IEEE 2010;1:173–80*.
- [14] Franca JGD, Gazziro MA, Ide AN, Saito JH. A 3D scanning system based on laser triangulation and variable field of view. *Image Process 2005 ICIP 2005 IEEE Int Conf On 2005;1 IEEE I–425*.
- [15] Sciammarella CA, Lamberti L, Boccaccio A. General model for moiré contouring, part 1: theory. *Opt Eng* 2008;47:033605.
- [16] Takeda M, Ina H, Kobayashi S. Fourier-transform method of fringe-pattern analysis for computer-based topography and interferometry. *J Opt Soc Am* 1982;72:156. doi:10.1364/JOSA.72.000156.
- [17] Su X, Chen W. Fourier transform profilometry: a review. *Opt Lasers Eng* 2001;22.
- [18] Qian K. Windowed Fourier transform for fringe pattern analysis. *Appl Opt* 2004;43:2695–702. doi:10.1364/AO.43.002695.
- [19] Zuo C, Feng S, Huang L, Tao T, Yin W, Chen Q. Phase shifting algorithms for fringe projection profilometry: a review. *Opt Lasers Eng* 2018;109:23–59. doi:10.1016/j.optlaseng.2018.04.019.
- [20] Wang Z, Du H, Park S, Xie H. Three-dimensional shape measurement with a fast and accurate approach. *Appl Opt* 2009;48:1052–61.
- [21] High-resolution Huang PS. real-time three-dimensional shape measurement. *Opt Eng* 2006;45:123601. doi:10.1117/1.2402128.
- [22] Huang PS. Novel method for structured light system calibration. *Opt Eng* 2006;45:083601. doi:10.1117/1.2336196.
- [23] Kowarschik RM, Kuehmstedt P, Gerber J, Schreiber W, Notni G. Adaptive optical 3-D-measurement with structured light. *Opt Eng* 2000;39.
- [24] Schreiber W, Notni G. Theory and arrangements of self-calibrating whole-body 3-D-measurement systems using fringe projection technique. *Opt Eng* 2000;39.
- [25] Hu Y, Chen Q, Feng S, Tao T, Li H, Zuo C. Real-time microscopic 3D shape measurement based on optimized pulse-width-modulation binary fringe projection. *Meas Sci Technol* 2017;28:075010. doi:10.1088/1361-6501/aa7277.
- [26] Sun J, Zuo C, Feng S, Yu S, Zhang Y, Chen Q. Improved intensity-optimized dithering technique for 3D shape measurement. *Opt Lasers Eng* 2015;66:158–64. doi:10.1016/j.optlaseng.2014.09.008.
- [27] Ayubi GA, Ayubi JA, Martino JMD, Ferrari JA. Pulse-width modulation in defocused three-dimensional fringe projection. *Opt Lett* 2010;35:3682–4. doi:10.1364/OL.35.003682.
- [28] Zuo C, Chen Q, Feng S, Feng F, Gu G, Sui X. Optimized pulse width modulation pattern strategy for three-dimensional profilometry with projector defocusing. *Appl Opt* 2012;51:4477. doi:10.1364/AO.51.004477.
- [29] Wang Y, Zhang S. Comparison of the squared binary, sinusoidal pulse width modulation, and optimal pulse width modulation methods for three-dimensional shape measurement with projector defocusing. *Appl Opt* 2012;51:861–72. doi:10.1364/AO.51.000861.
- [30] Zhang S. Flexible 3D shape measurement using projector defocusing: extended measurement range. *Opt Lett* 2010;35:934. doi:10.1364/OL.35.000934.
- [31] Sansoni G, Carocci M, Rodella R. Three-dimensional vision based on a combination of gray-code and phase-shift light projection: analysis and compensation of the systematic errors. *Appl Opt* 1999;38:6565–73. doi:10.1364/AO.38.006565.
- [32] Zhang M, Chen Q, Tao T, Feng S, Hu Y, Li H, et al. Robust and efficient multi-frequency temporal phase unwrapping: optimal fringe frequency and pattern sequence selection. *Opt Express* 2017;25:20381. doi:10.1364/OE.25.020381.
- [33] Li H, Hu Y, Tao T, Feng S, Zhang M, Zhang Y, et al. Optimal wavelength selection strategy in temporal phase unwrapping with projection distance minimization. *Appl Opt* 2018;57:2352. doi:10.1364/AO.57.002352.
- [34] Van der Jeught S, Dirckx JJJ. Real-time structured light profilometry: a review. *Opt Lasers Eng* 2016;87:18–31. doi:10.1016/j.optlaseng.2016.01.011.
- [35] Zuo C, Tao T, Feng S, Huang L, Asundi A, Chen Q. Micro Fourier Transform Profilometry (μ FTP): 3D shape measurement at 10,000 frames per second. *Opt Lasers Eng* 2018;102:70–91. doi:10.1016/j.optlaseng.2017.10.013.
- [36] Zuo C, Chen Q, Gu G, Feng S, Feng F. High-speed three-dimensional profilometry for multiple objects with complex shapes. *Opt Express* 2012;20:19493. doi:10.1364/OE.20.019493.
- [37] Heist S, Kühmstedt P, Tünnermann A, Notni G. Theoretical considerations on aperiodic sinusoidal fringes in comparison to phase-shifted sinusoidal fringes for high-speed three-dimensional shape measurement. *Appl Opt* 2015;54:10541–51. doi:10.1364/AO.54.010541.
- [38] Zhang S. Recent progresses on real-time 3D shape measurement using digital fringe projection techniques. *Opt Lasers Eng* 2010;48:149–58. doi:10.1016/j.optlaseng.2009.03.008.
- [39] Qi Z, Wang Z, Huang J, Xing C, Gao J. Error of image saturation in the structured-light method. *Appl Opt* 2018;57:A181. doi:10.1364/AO.57.00A181.
- [40] Long J, Xi J, Zhang J, Zhu M, Cheng W, Li Z, et al. Recovery of absolute phases for the fringe patterns of three selected wavelengths with improved anti-error capability. *J Mod Opt* 2016;63:1695–705.
- [41] Van der Jeught S. Real-time geometric lens distortion correction using a graphics processing unit. *Opt Eng* 2012;51:027002. doi:10.1117/1.OE.51.2.027002.
- [42] Peng J, Wang M, Deng D, Liu X, Yin Y, Peng X. Distortion correction for microscopic fringe projection system with Scheimpflug telecentric lens. *Appl Opt* 2015;54:10055. doi:10.1364/AO.54.010055.
- [43] Li K, Bu J, Zhang D. Lens distortion elimination for improving measurement accuracy of fringe projection profilometry. *Opt Lasers Eng* 2016;85:53–64. doi:10.1016/j.optlaseng.2016.04.009.
- [44] Precise Industrial 3D Metrology. GOM n.d. <https://www.gom.com/> (accessed November 24, 2019).
- [45] Polyga - 3D Scanning Technologies for Professionals. Polyga n.d. <https://www.polyga.com/> (accessed November 24, 2019).
- [46] Howard V, Reed M, Reed M. Unbiased stereology: three-dimensional measurement in microscopy. Garland Sci 2004. doi:10.4324/9780203006399.
- [47] Gardner JW, Varadan VK. Microsensors, mems and smart devices. New York, NY, USA: John Wiley & Sons, Inc.; 2001.
- [48] Leonhardt K, Droste U, Tiziani HJ. Microshape and rough-surface analysis by fringe projection. *Appl Opt* 1994;33:12.
- [49] Windecker R, Fleischer M, Tiziani H. Three-dimensional topometry with stereo microscopes. *Opt Eng* 1997;36:3372. doi:10.1117/1.601576.
- [50] Quan C, He XY, Wang CF, Tay CJ, Shang HM. Shape measurement of small objects using LCD fringe projection with phase shifting. *Opt Commun* 2001;189:21–9. doi:10.1016/S0030-4018(01)01038-0.
- [51] Zhang C, Huang PS, Chiang F-P. Microscopic phase-shifting profilometry based on digital micromirror device technology. *Appl Opt* 2002;41:5896. doi:10.1364/AO.41.005896.

- [52] Li A, Peng X, Yin Y, Liu X, Zhao Q, Körner K, et al. Fringe projection based quantitative 3D microscopy. *Opt - Int J Light Electron Opt* 2013;124:5052–6. doi:10.1016/j.jleleo.2013.03.070.
- [53] Proll K-P, Nivet J-M, Körner K, Tiziani HJ. Microscopic three-dimensional topometry with ferroelectric liquid-crystal-on-silicon displays. *Appl Opt* 2003;42:1773. doi:10.1364/AO.42.001773.
- [54] DLP Overview | DLP Products | TI.com n.d. <http://www.ti.com/dlp-chip/overview.html> (accessed August 8, 2019).
- [55] Zhang Z. A flexible new technique for camera calibration. *IEEE Trans Pattern Anal Mach Intell* 2000;22:1330–4. doi:10.1109/34.888718.
- [56] Hu Y, Chen Q, Feng S, Tao T, Asundi A, Zuo C. A new microscopic telecentric stereo vision system - calibration, rectification, and three-dimensional reconstruction. *Opt Lasers Eng* 2019;113:14–22. doi:10.1016/j.optlaseng.2018.09.011.
- [57] Li B, Zhang S. Flexible calibration method for microscopic structured light system using telecentric lens. *Opt Express* 2015;23:25795. doi:10.1364/OE.23.025795.
- [58] Hu Y, Chen Q, Tao T, Li H, Zuo C. Absolute three-dimensional micro surface profile measurement based on a greenough-type stereomicroscope. *Meas Sci Technol* 2017;28:045004. doi:10.1088/1361-6501/aa5a2d.
- [59] Li D, Liu C, Tian J. Telecentric 3D profilometry based on phase-shifting fringe projection. *Opt Express* 2014;22:31826. doi:10.1364/OE.22.031826.
- [60] Zhu F, Liu W, Shi H, He X. Accurate 3D measurement system and calibration for speckle projection method. *Opt Lasers Eng* 2010;48:1132–9. doi:10.1016/j.optlaseng.2009.12.016.
- [61] Zuo C, Chen Q, Feng S, Gu G, Asundi A. Real-time three-dimensional infrared imaging using fringe projection profilometry. *Chin Opt Lett* 2013;11 S21101–S21104. doi:10.3788/COL201311.S21101.
- [62] Zhong K, Li Z, Zhou X, Zhan G, Liu X, Shi Y, et al. Real-time 3D shape measurement system with full temporal resolution and spatial resolution. *Three-Dimens Image Process Meas 3DIPM Appl* 2014:901309.
- [63] Tao T, Chen Q, Da J, Feng S, Hu Y, Zuo C. Real-time 3-D shape measurement with composite phase-shifting fringes and multi-view system. *Opt Express* 2016;24:20253. doi:10.1364/OE.24.020253.
- [64] Li B, Zhang S. Microscopic structured light 3D profilometry: binary defocusing technique vs. sinusoidal fringe projection. *Opt Lasers Eng* 2017;96:117–23. doi:10.1016/j.optlaseng.2016.06.009.
- [65] Zhang Q, Su X. High-speed optical measurement for the drumhead vibration. *Opt Express* 2005;13:3110–16. doi:10.1364/OPEX.13.003110.
- [66] Creath K. Step height measurement using two-wavelength phase-shifting interferometry. *Appl Opt* 1987;26:2810–16. doi:10.1364/AO.26.002810.
- [67] Körner K. One-grating projection for absolute three-dimensional profiling. *Opt Eng* 2001;40:1653. doi:10.1117/1.1385509.
- [68] Scheffer TJ, Nehring J. A new, highly multiplexable liquid crystal display. *Appl Phys Lett* 1984;45:1021–3. doi:10.1063/1.95048.
- [69] Dudley D, Duncan WM, Slaughter J. Emerging digital micromirror device (DMD) applications. *MOEMS disp. imaging syst.. Int Soc Opt Photonics* 2003;4985:14–25. doi:10.1117/12.480761.
- [70] Wolfe JE, Chipman RA. Polarimetric characterization of liquid-crystal-on-silicon panels. *Appl Opt* 2006;45:1688–703. doi:10.1364/AO.45.001688.
- [71] Proll K-P, Nivet J-M, Voland C, Tiziani HJ. Application of a liquid-crystal spatial light modulator for brightness adaptation in microscopic topometry. *Appl Opt* 2000;39:6430. doi:10.1364/AO.39.006430.
- [72] Chen L-C, Liao C-C, Lai M-J. Full-field micro surface profilometry using digital fringe projection with spatial encoding principle. *J Phys Conf Ser* 2005;13:147–50. doi:10.1088/1742-6596/13/1/034.
- [73] Hu Y, Chen Q, Zhang Y, Feng S, Tao T, Li H, et al. Dynamic microscopic 3D shape measurement based on marker-embedded Fourier transform profilometry. *Appl Opt* 2018;57:772. doi:10.1364/AO.57.000772.
- [74] Hu Y, Liang Y, Tao T, Feng S, Zuo C, Zhang Y, et al. Dynamic 3D measurement of thermal deformation based on geometric-constrained stereo-matching with a stereo microscopic system. *Meas Sci Technol* 2019;30:125007. doi:10.1088/1361-6501/ab35a1.
- [75] Yu Y, Huang S, Zhang Z, Gao F, Jiang X. In: Czarske J, Zhang S, Sampson D, Wang W, Liao Y, editors; 2014. p. 92972. doi:10.1117/12.2073051.
- [76] Van der Jeught S, Soons JAM, Dirckx JJJ. Real-time microscopic phase-shifting profilometry. *Appl Opt* 2015;54:4953. doi:10.1364/AO.54.004953.
- [77] Quan C, Tay CJ, He XY, Kang X, Shang HM. Microscopic surface contouring by fringe projection method. *Opt Laser Technol* 2002;34:547–52. doi:10.1016/S0030-3992(02)00070-1.
- [78] Wang WH, Wong YS, Hong GS. 3D measurement of crater wear by phase shifting method. *Wear* 2006;261:164–71. doi:10.1016/j.wear.2005.09.036.
- [79] Chen J, Guo T, Wang L, Wu Z, Fu X, Hu X. In: Lin J, editor; 2013. editor p. 87594. doi:10.1117/12.2014756.
- [80] Yin Y, Wang M, Gao BZ, Liu X, Peng X. Fringe projection 3D microscopy with the general imaging model. *Opt Express* 2015;23:6846. doi:10.1364/OE.23.006846.
- [81] Liu H, Lin H, Yao L. Calibration method for projector-camera-based telecentric fringe projection profilometry system. *Opt Express* 2017;25:31492–508. doi:10.1364/OE.25.031492.
- [82] Wang M, Yin Y, Deng D, Meng X, Liu X, Peng X. Improved performance of multi-view fringe projection 3D microscopy. *Opt Express* 2017;25:19408. doi:10.1364/OE.25.019408.
- [83] Hartley R, Zisserman A. *Multiple view geometry in computer vision. 2 edition.* Cambridge, UK: New York: Cambridge University Press; 2004.
- [84] Yao L, Liu H. A flexible calibration approach for cameras with double-sided telecentric lenses. *Int J Adv Robot Syst* 2016;13:82. doi:10.5772/63825.
- [85] Li D, Tian J. An accurate calibration method for a camera with telecentric lenses. *Opt Lasers Eng* 2013;51:538–41. doi:10.1016/j.optlaseng.2012.12.008.
- [86] Guan B, Yao L, Liu H, Shang Y. An accurate calibration method for non-overlapping cameras with double-sided telecentric lenses. *Opt - Int J Light Electron Opt* 2017;131:724–32. doi:10.1016/j.jleleo.2016.11.156.
- [87] Haskamp K, Kästner M, Reithmeier E. Accurate calibration of a fringe projection system by considering telecentricity. In: Lehmann PH, Osten W, Gasteringer K, editors., 2011, p. 80821B. doi:10.1117/12.888037.
- [88] Huiyang L, Zhong C, Xianmin Z. Calibration of camera with small FOV and DOF telecentric lens. *IEEE* 2013:498–503. doi:10.1109/ROBIO.2013.6739509.
- [89] Hu Y, Feng S, Tao T, Zuo C, Chen Q, Asundi A. Calibration of telecentric cameras with distortion center estimation. Sixth int. conf. opt. photonic eng. ICOPEN 2018. *Int Soc Opt Photonics* 2018;10827:1082720.
- [90] Rao L, Da F, Kong W, Huang H. Flexible calibration method for telecentric fringe projection profilometry systems. *Opt Express* 2016;24:1222–37. doi:10.1364/OE.24.001222.
- [91] Zhang S, Li B, Ren F, Dong R. High-precision measurement of binocular telecentric vision system with novel calibration and matching methods. *IEEE Access* 2019;7:54682–92. doi:10.1109/ACCESS.2019.2913181.
- [92] Chen Z, Liao H, Zhang X. Telecentric stereo micro-vision system: calibration method and experiments. *Opt Lasers Eng* 2014;57:82–92. doi:10.1016/j.optlaseng.2014.01.021.
- [93] Li Z, Zhong K, Li YF, Zhou X, Shi Y. Multiview phase shifting: a full-resolution and high-speed 3D measurement framework for arbitrary shape dynamic objects. *Opt Lett* 2013;38:1389–91.
- [94] Dhond UR, Aggarwal JK. Structure from stereo-a review. *IEEE Trans Syst Man Cybern* 1989;19:1489–510. doi:10.1109/21.44067.
- [95] Guo H. Least-squares calibration method for fringe projection profilometry. *Opt Eng* 2005;44:033603. doi:10.1117/1.1871832.
- [96] Bruning JH, Herriott DR, Gallagher JE, Rosenfeld DP, White AD, Brangaccio DJ. Digital wavefront measuring interferometer for testing optical surfaces and lenses n.d.:11.
- [97] Lin JF, Su X. Two-dimensional Fourier transform profilometry for the automatic measurement of three-dimensional object shapes. *Opt Eng* 1990;29:64–6.
- [98] Podder P, Zaman Khan T, Haque Khan M, Mukhtadir Rahman M. Comparative performance analysis of hamming, hanning and blackman window. *Int J Comput Appl* 2014;96:1–7. doi:10.5120/16891-6927.
- [99] Su X, Zhang Q. Dynamic 3-D shape measurement method: a review. *Opt Lasers Eng* 2010;48:191–204. doi:10.1016/j.optlaseng.2009.03.012.
- [100] Srinivasan V, Liu HC, Hallioua M. Automated phase-measuring profilometry of 3-D diffuse objects. *Appl Opt* 1984;23:3105–8. doi:10.1364/AO.23.003105.
- [101] Huang PS, Hu QJ, Chiang F-P. Double three-step phase-shifting algorithm. *Appl Opt* 2002;41:4503–9. doi:10.1364/AO.41.004503.
- [102] Hariharan P, Oreb BF, Eiju T. Digital phase-shifting interferometry: a simple error-compensating phase calculation algorithm. *Appl Opt* 1987;26:2504–6. doi:10.1364/AO.26.002504.
- [103] Zhang S, Yau S-T. High-speed three-dimensional shape measurement system using a modified two-plus-one phase-shifting algorithm. *Opt Eng* 2007;46:113603. doi:10.1117/1.2147311.
- [104] Huang PS, Zhang S, Chiang F-P. Trapezoidal phase-shifting method for three-dimensional shape measurement. *Opt Eng* 2005;44:123601. doi:10.1117/1.2147311.
- [105] Jia P, Kofman J, English CE. Two-step triangular-pattern phase-shifting method for three-dimensional object-shape measurement. *Opt Eng* 2007;46:083201. doi:10.1117/1.2768616.
- [106] Li J, Su X, Guo L. Improved Fourier transform profilometry for the automatic measurement of three-dimensional object shapes. *Opt Eng* 1990;29:1439–45. doi:10.1117/12.55746.
- [107] Servin M, Estrada JC, Quiroga JA. The general theory of phase shifting algorithms. *Opt Express* 2009;17:21867. doi:10.1364/OE.17.021867.
- [108] Lai G, Yatagai T. Generalized phase-shifting interferometry. *JOSA A* 1991;8:822–7. doi:10.1364/JOSA.8.000822.
- [109] Zuo C, Huang L, Zhang M, Chen Q, Asundi A. Temporal phase unwrapping algorithms for fringe projection profilometry: A comparative review. *Opt Lasers Eng* 2016;85:84–103. doi:10.1016/j.optlaseng.2016.04.022.
- [110] Abdel-Aziz YI, Karara HM. Direct linear transformation from comparator coordinates into object space coordinates in close-range photogrammetry. *Photogramm Eng Remote Sens* 2015;81:103–7. doi:10.14358/PERS.81.2.103.
- [111] Tsai R. A versatile camera calibration technique for high-accuracy 3D machine vision metrology using off-the-shelf TV cameras and lenses. *IEEE J Robot Autom* 1987;3:323–44. doi:10.1109/JRA.1987.1087109.
- [112] Tsai RY. An efficient and accurate camera calibration technique for 3D machine vision. *Proc IEEE Conf on Comput Vis Pattern Recognit* 1986:364–74.
- [113] Liu H, Su W-H, Reichard K, Yin S. Calibration-based phase-shifting projected fringe profilometry for accurate absolute 3D surface profile measurement. *Opt Commun* 2003;216:65–80. doi:10.1016/S0030-4018(02)02290-3.
- [114] Wang Z, Nguyen DA, Barnes JC. Some practical considerations in fringe projection profilometry. *Opt Lasers Eng* 2010;48:218–25. doi:10.1016/j.optlaseng.2009.06.005.
- [115] Huang L, Chua PSK, Asundi A. Least-squares calibration method for fringe projection profilometry considering camera lens distortion. *Appl Opt* 2010;49:1539. doi:10.1364/AO.49.001539.
- [116] Zhang Z, Ma H, Guo T, Zhang S, Chen J. Simple, flexible calibration of phase calculation-based three-dimensional imaging system. *Opt Lett* 2011;36:1257. doi:10.1364/OL.36.001257.
- [117] Du H, Wang Z. Three-dimensional shape measurement with an arbitrarily arranged fringe projection profilometry system. *Opt Lett* 2007;32:2438. doi:10.1364/OL.32.002438.

- [118] Tanaka H, Sumi Y, Matsumoto Y. A solution to pose ambiguity of visual markers using Moiré patterns. IEEE 2014;3129–34. doi:10.1109/IROS.2014.6942995.
- [119] Bergach MA, Kofman E, de Simone R, Tissot S, Syska M. Efficient FFT mapping on GPU for radar processing application: modeling and implementation. ArXiv150508067 Cs 2015.
- [120] Feng S, Chen Q, Zuo C. Graphics processing unit-assisted real-time three-dimensional measurement using speckle-embedded fringe. Appl Opt 2015;54:6865. doi:10.1364/AO.54.006865.
- [121] Mittal S, Vetter JS. A survey of CPU-GPU heterogeneous computing techniques. ACM Comput Surv 2015;47:1–35. doi:10.1145/2788396.
- [122] Zhang S, Royer D, Yau S-T. GPU-assisted high-resolution, real-time 3-D shape measurement. Opt Express 2006;14:9120–9. doi:10.1364/OE.14.009120.
- [123] Feng S, Chen Q, Zuo C, Sun J, Yu SL. High-speed real-time 3-D coordinates measurement based on fringe projection profilometry considering camera lens distortion. Opt Commun 2014;329:44–56. doi:10.1016/j.optcom.2014.04.067.
- [124] Zhang S, Huang PS. Phase error compensation for a 3-D shape measurement system based on the phase-shifting method. Opt Eng 2007;46:063601. doi:10.1117/1.2746814.
- [125] Zhong J, Wang M. Phase unwrapping by lookup table method: application to phase map with singular points. Opt Eng 1999;38. doi:10.1117/1.602314.
- [126] Zhang S, Yau S-T. Generic nonsinusoidal phase error correction for three-dimensional shape measurement using a digital video projector. Appl Opt 2007;46:36–43. doi:10.1364/AO.46.000036.
- [127] Zuo C, Chen Q, Gu G, Feng S, Feng F, Li R, et al. High-speed three-dimensional shape measurement for dynamic scenes using bi-frequency tripolar pulse-width-modulation fringe projection. Opt Lasers Eng 2013;51:953–60. doi:10.1016/j.optlaseng.2013.02.012.
- [128] Feng S, Zhang Y, Chen Q, Zuo C, Li R, Shen G. General solution for high dynamic range three-dimensional shape measurement using the fringe projection technique. Opt Lasers Eng 2014;59:56–71. doi:10.1016/j.optlaseng.2014.03.003.
- [129] Feng S, Chen Q, Zuo C, Li R, Shen G, Feng F. Automatic identification and removal of outliers for high-speed fringe projection profilometry. Opt Eng 2013;52:013605. doi:10.1117/1.OE.52.1.013605.
- [130] Su X-Y, Li J, Guo L-R, Su W-Y, Grover CP. An improved Fourier transform profilometry; 1989. editor. p. 241. doi:10.1117/12.947595.
- [131] Hu E, He Y. Surface profile measurement of moving objects by using an improved π phase-shifting Fourier transform profilometry. Opt Lasers Eng 2009;47:57–61. doi:10.1016/j.optlaseng.2008.08.003.
- [132] Guo H, Huang PS, Huang PS, Yoshizawa T, Harding KG. 3-D shape measurement by use of a modified Fourier transform method; 2008. editors p. 70660. doi:10.1117/12.798170.
- [133] CAI Z, LIU X, PENG X, YIN Y, LI A, WU J, et al. Structured light field 3D imaging n.d.:11.
- [134] Yau S-T. High dynamic range scanning technique. Opt Eng 2009;48:033604. doi:10.1117/1.3099720.
- [135] Zhao H, Liang X, Diao X, Jiang H. Rapid in-situ 3D measurement of shiny object based on fast and high dynamic range digital fringe projector. Opt Lasers Eng 2014;54:170–4. doi:10.1016/j.optlaseng.2013.08.002.
- [136] Hu E, He Y, Chen Y. Study on a novel phase-recovering algorithm for partial intensity saturation in digital projection grating phase-shifting profilometry. Opt - Int J Light Electron Opt 2010;121:23–8. doi:10.1016/j.ijleo.2008.05.010.
- [137] Hu E, He Y, Wu W. Further study of the phase-recovering algorithm for saturated fringe patterns with a larger saturation coefficient in the projection grating phase-shifting profilometry. Opt - Int J Light Electron Opt 2010;121:1290–4. doi:10.1016/j.ijleo.2009.01.007.
- [138] Chen Y, He Y, Hu E. Phase deviation analysis and phase retrieval for partial intensity saturation in phase-shifting projected fringe profilometry. Opt Commun 2008;281:3087–90. doi:10.1016/j.optcom.2008.01.070.
- [139] Hu Y, Chen Q, Liang Y, Feng S, Tao T, Zuo C. Microscopic 3D measurement of shiny surfaces based on a multi-frequency phase-shifting scheme. Opt Lasers Eng 2019;122:1–7. doi:10.1016/j.optlaseng.2019.05.019.
- [140] Morrison G. DLP vs LCD vs LCoS: projector tech pros and cons. CNET n.d. <https://www.cnet.com/news/dlp-vs-lcd-vs-lcos-projector-tech-pros-and-cons/> (accessed January 31, 2020).
- [141] Electropages. DLP vs. LCD vs. LED vs. LCoS vs. laser: shedding light on projector technology n.d. <https://www.electropages.com/blog/2019/06/dlp-vs-lcd-vs-led-vs-lcos-vs-laser-shedding-light-projector-technology> (accessed January 31, 2020).
- [142] DLP vs LCD vs LCoS Projector: Which should you buy? n.d. <http://projectorsavvy.com/dlp-vs-lcd-vs-lcos-projector-differences/> (accessed January 31, 2020).
- [143] Li B, Gibson J, Middendorf J, Wang Y, Zhang S, Harding KG, Huang PS, Yoshizawa T, editors; 2013. editors. San Diego, California, United States. doi:10.1117/12.2022225.